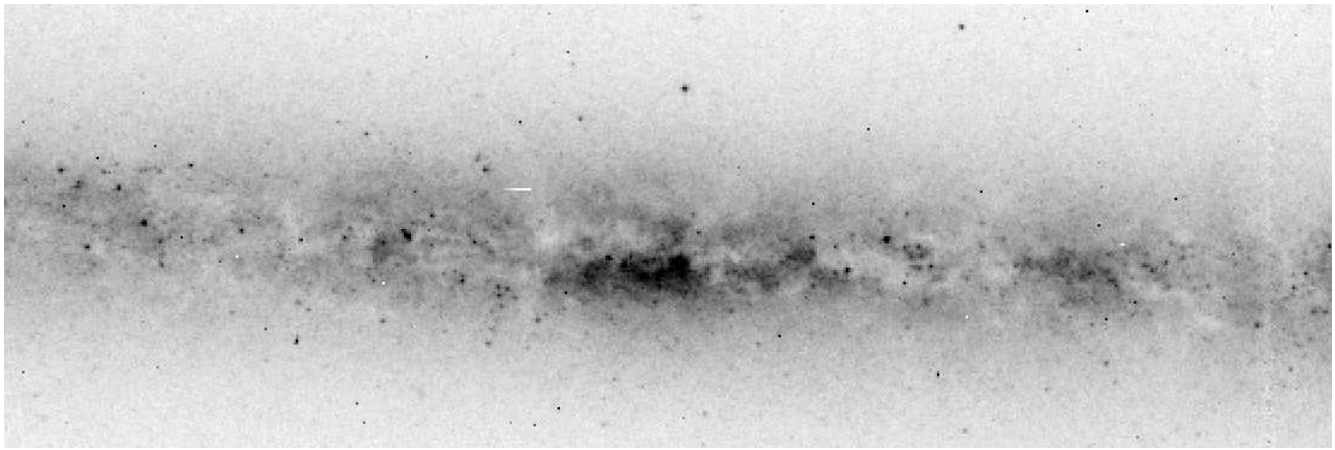

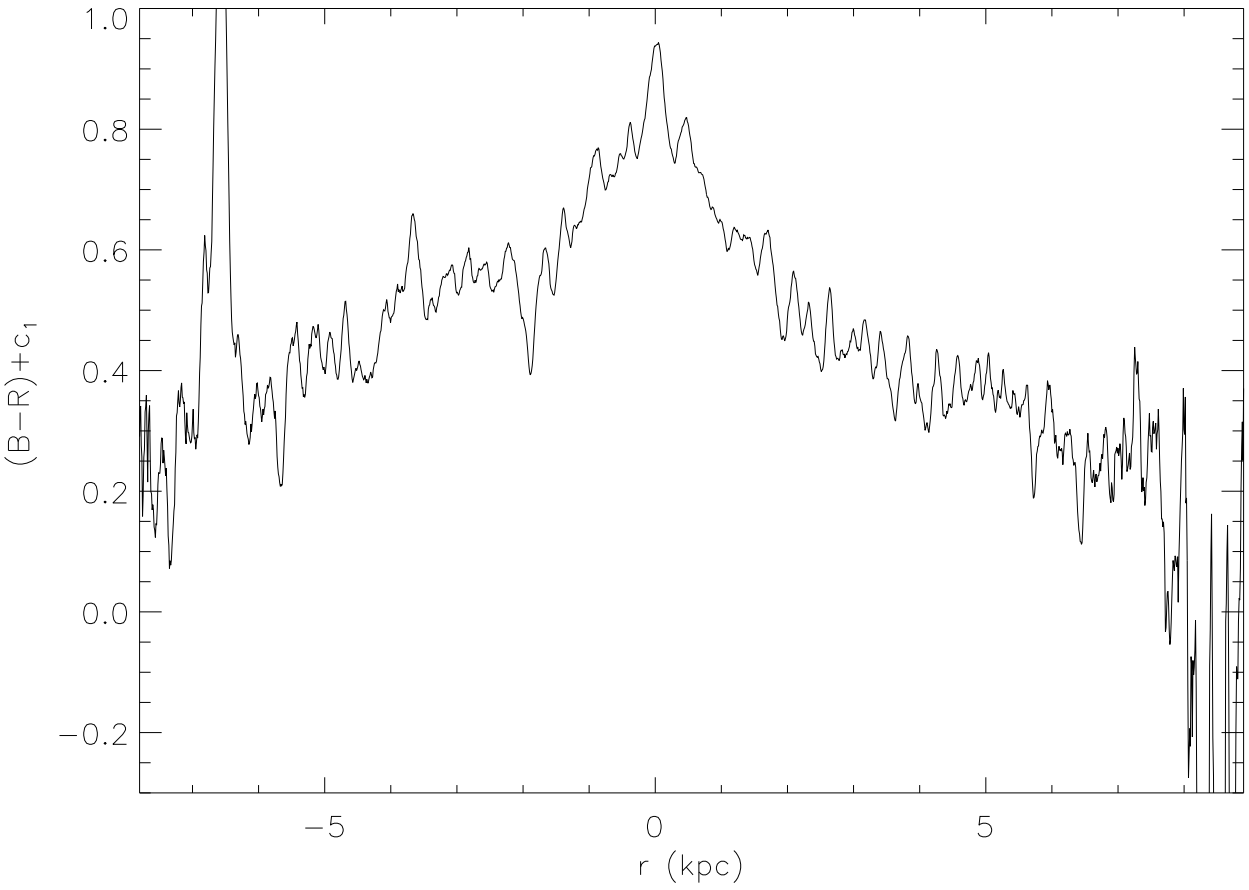
1.0
0.8
0.6
0.4
0.2
0.0
−0.2
(B−R)+c1
−5
0
5
r (kpc)

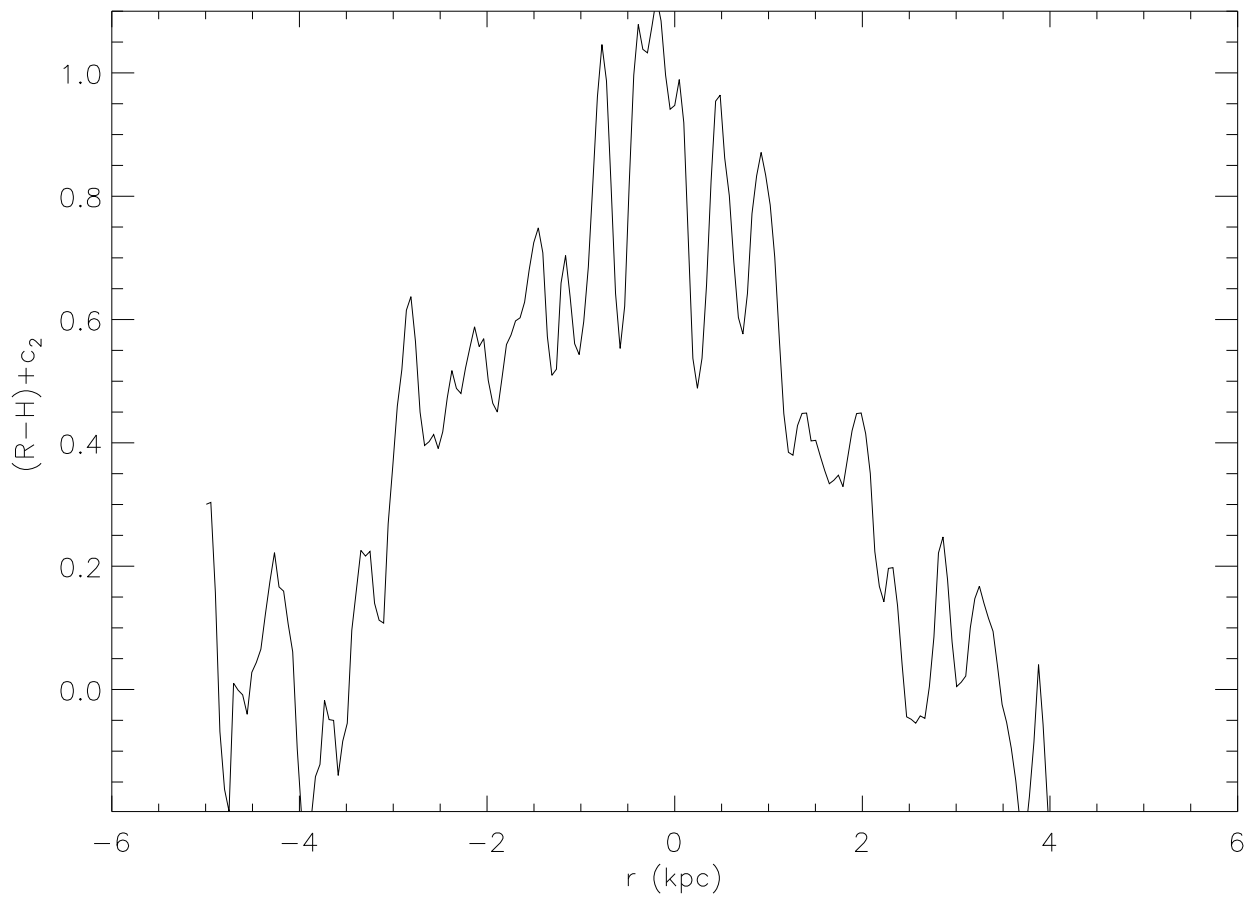
1.0
0.8
0.6
0.4
0.2
0.0
(R−H)+c2
−6
−4
−2
0
2
4
6
r (kpc)

This figure "Fig4.gif" is available in "gif" format from:

http://arXiv.org/ps/astro-ph/0010033v1

This figure "Fig5.gif" is available in "gif" format from:

http://arXiv.org/ps/astro-ph/0010033v1

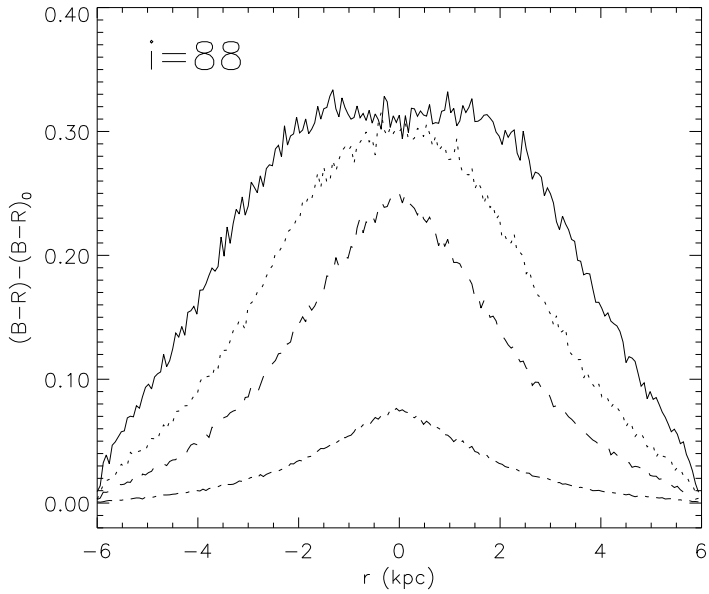
i=88
(B−R)−(B−R)0
r (kpc)

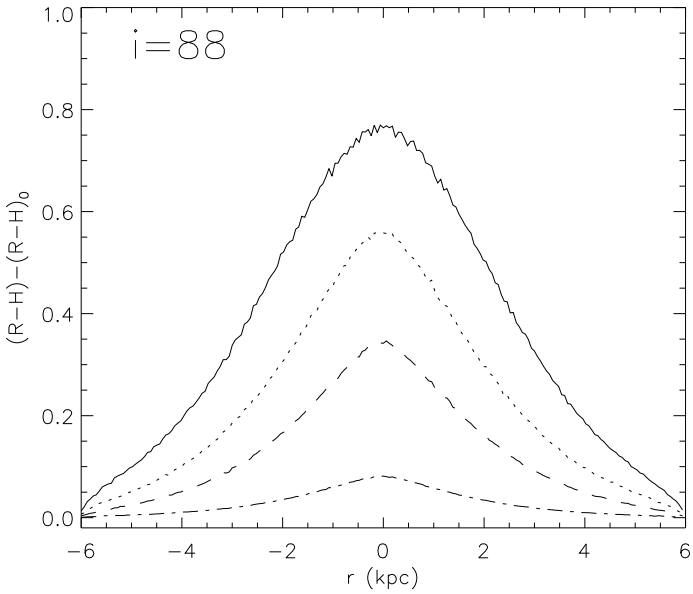
i=88
(R−H)−(R−H)0
r (kpc)

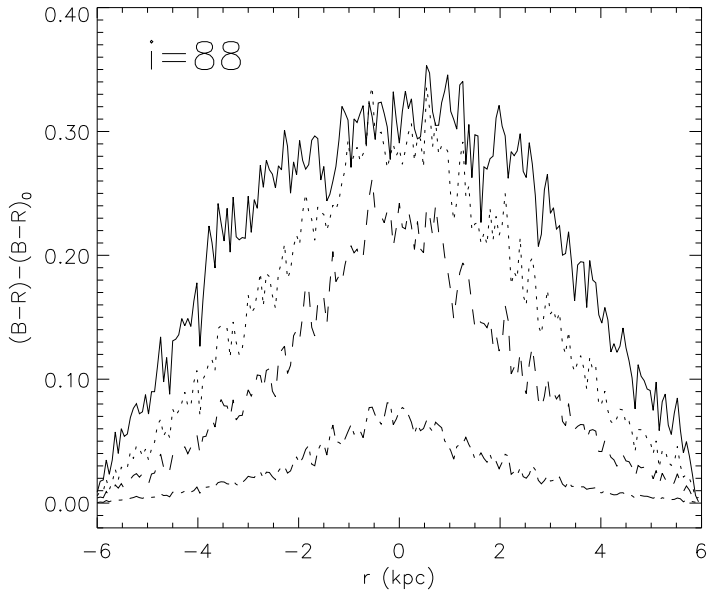
i=88
(B−R)−(B−R)0
r (kpc)

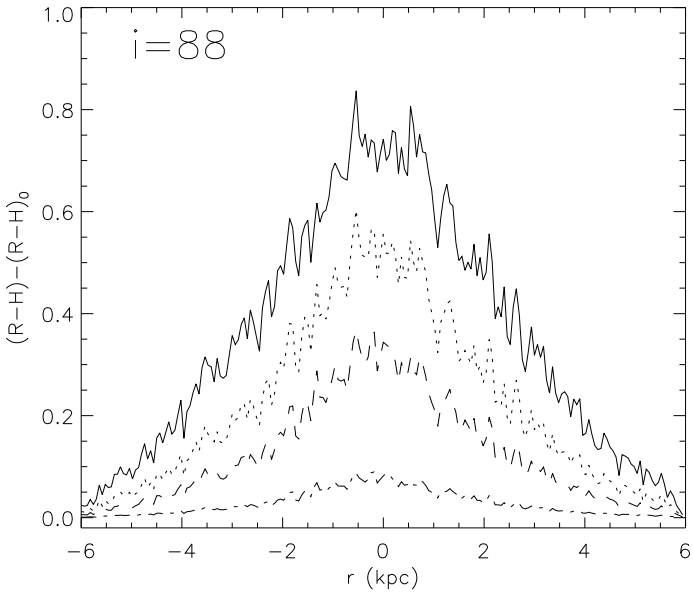
i=88
(R−H)−(R−H)0
r (kpc)

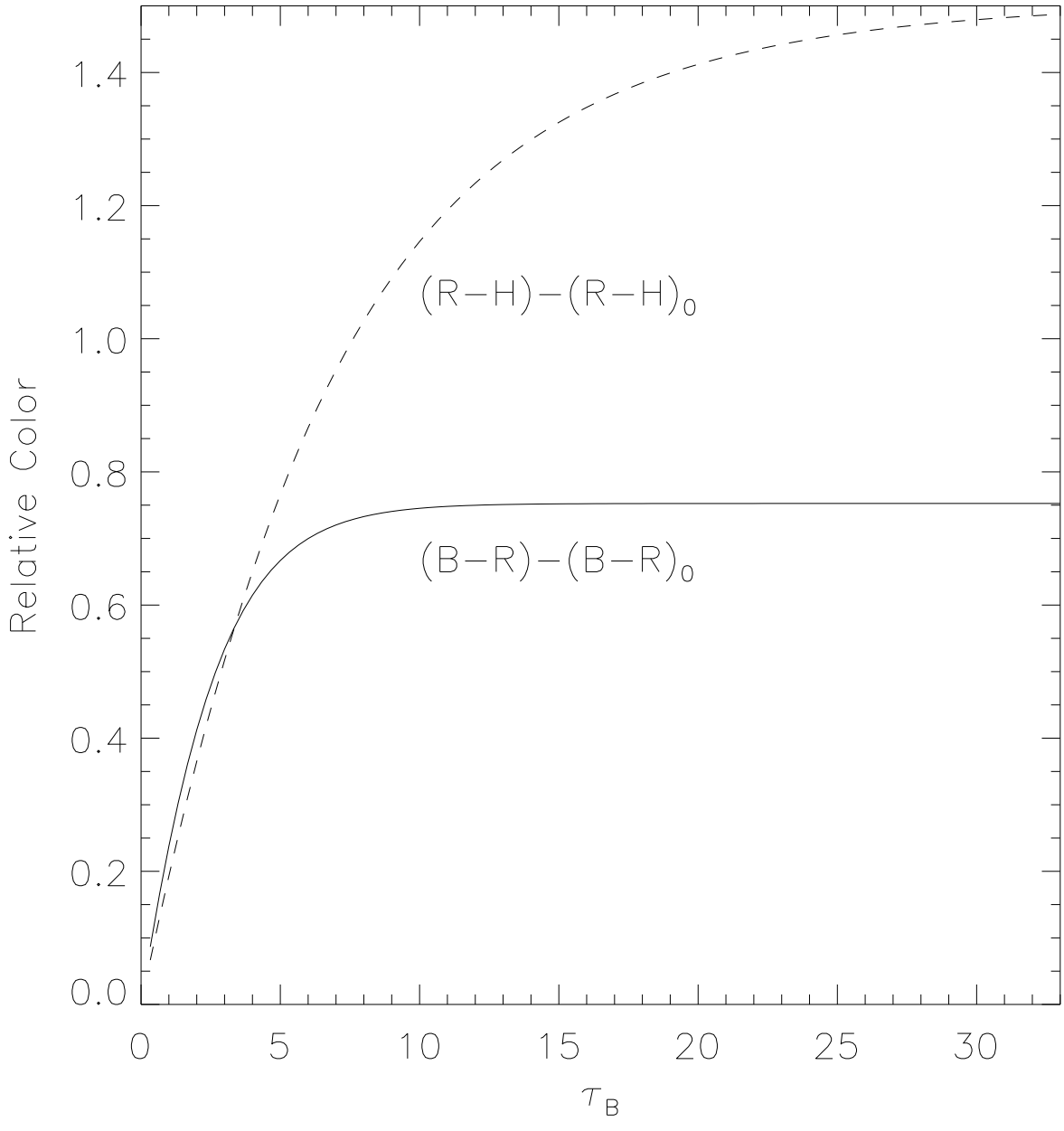
Relative Color
1.4
1.2
1.0
0.8
0.6
0.4
0.2
0.0
0
5
10
15
20
25
30
τ_B
$(R-H)-(R-H)_0$
$(B-R)-(B-R)_0$

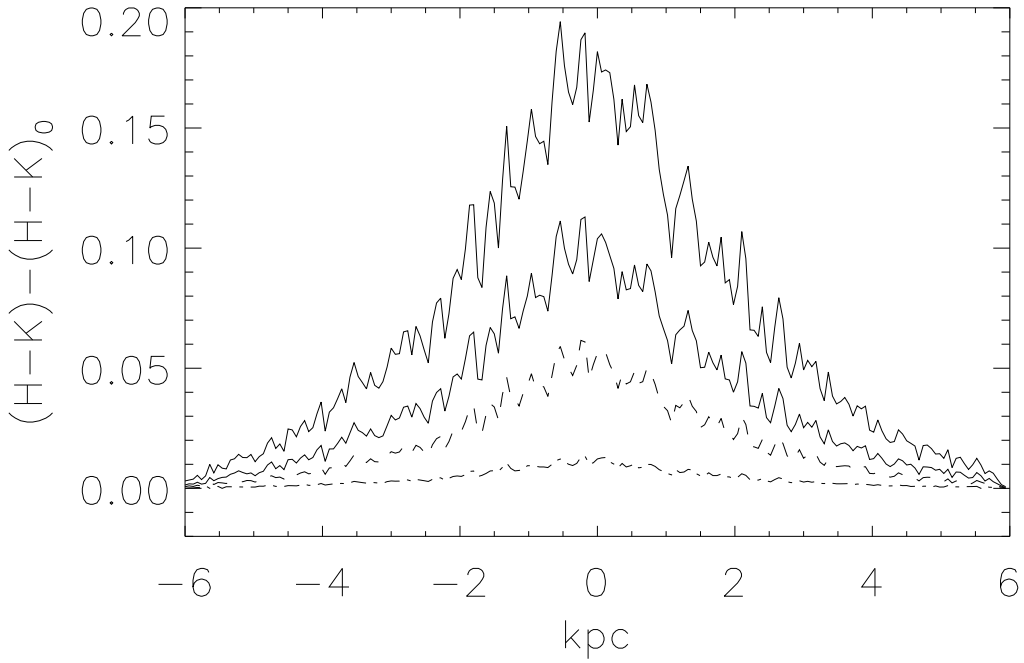
0.20
0.15
0.10
0.05
0.00
(H−K)−(H−K)o
−6
−4
−2
0
2
4
6
kpc

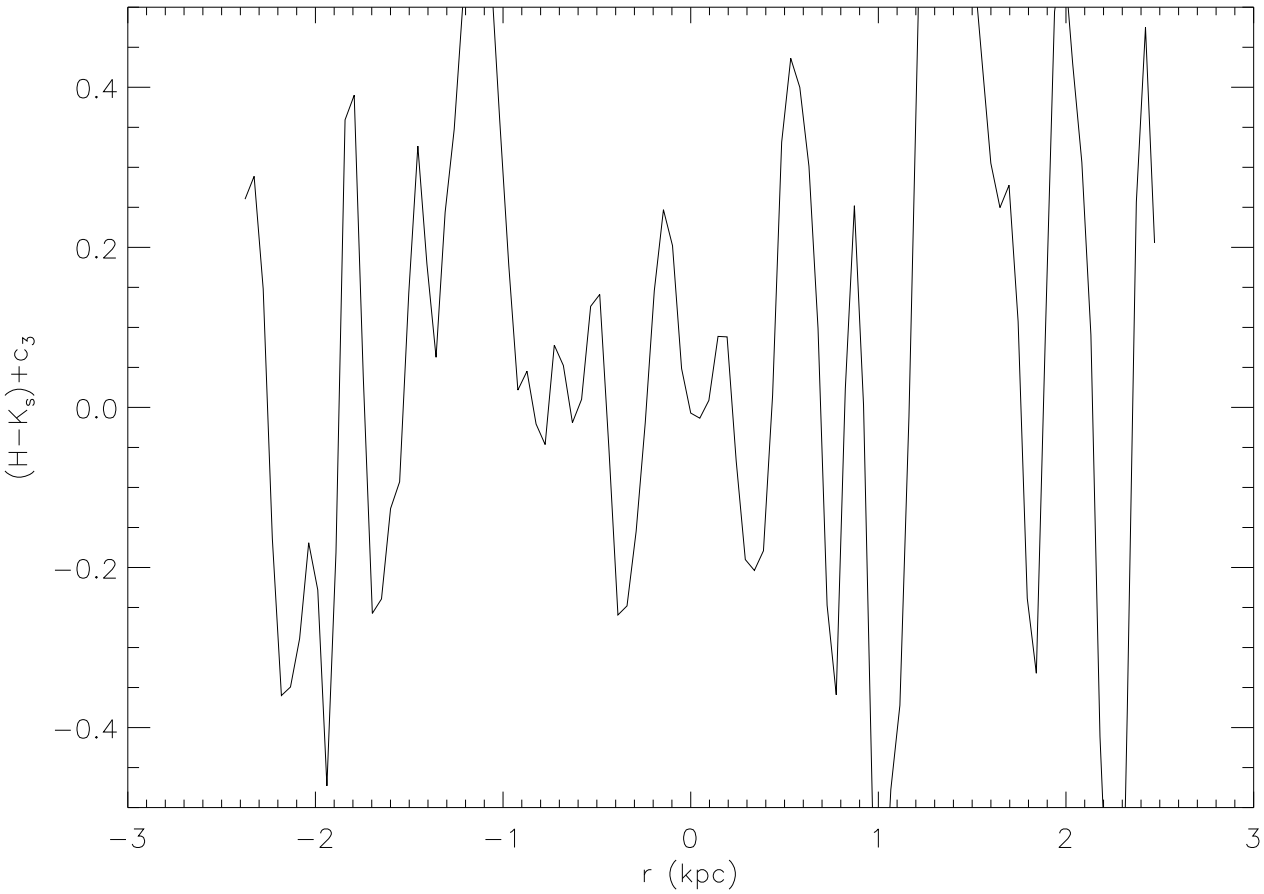
0.4
0.2
0.0
−0.2
−0.4
−3
−2
−1
0
1
2
3
r (kpc)
(H−K_s)+c_3

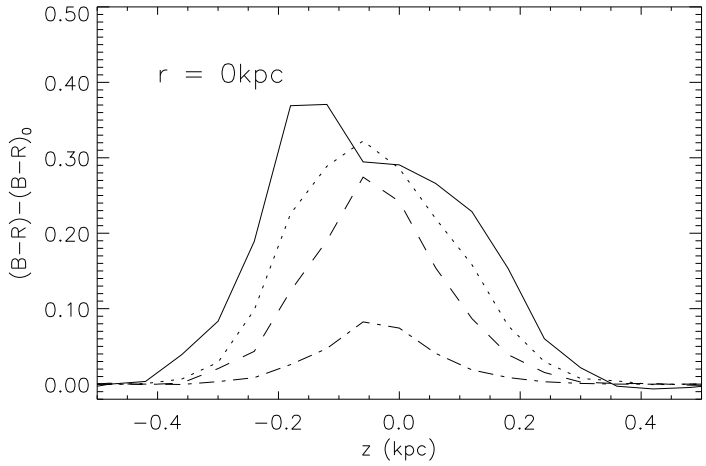
r = 0kpc
(B−R)−(B−R)0
z (kpc)

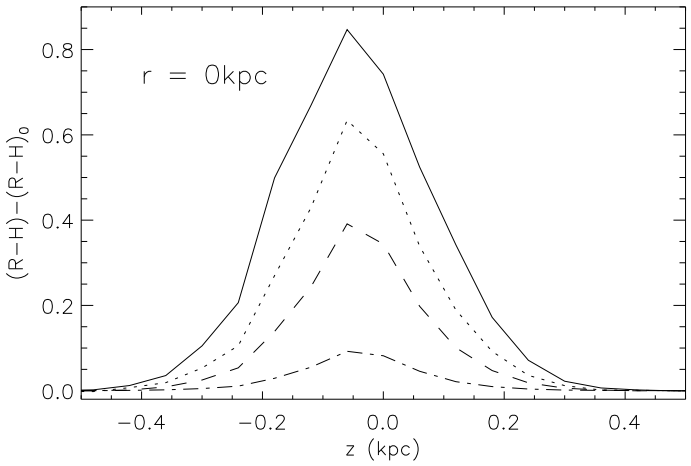
r = 0kpc
(R−H)−(R−H)0
z (kpc)

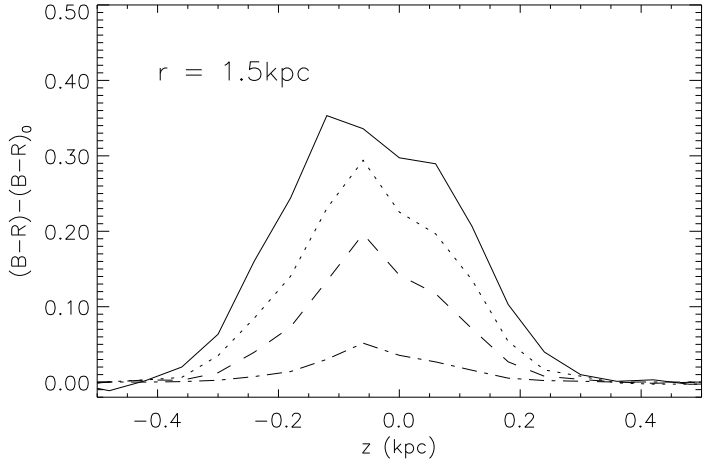
r = 1.5kpc
(B−R)−(B−R)0
z (kpc)

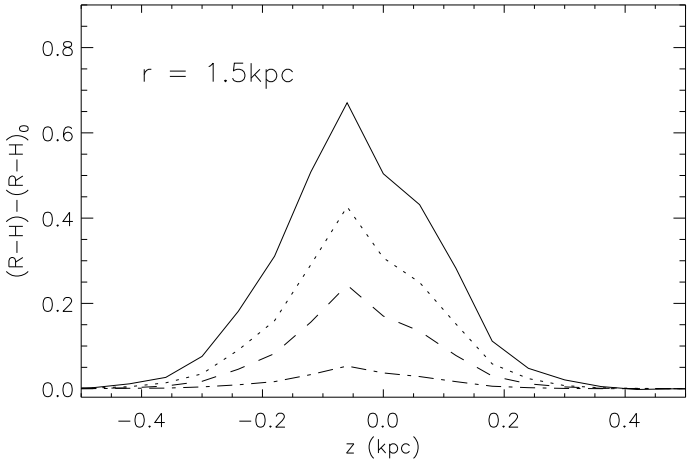
r = 1.5kpc
(R−H)−(R−H)0
z (kpc)

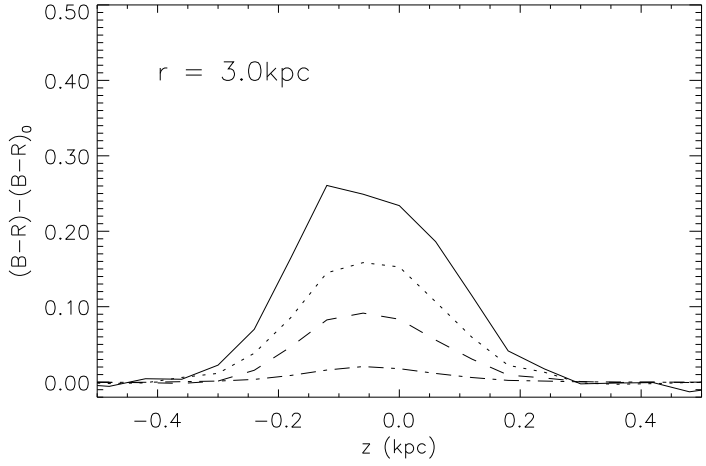
r = 3.0kpc
(B−R)−(B−R)0
z (kpc)

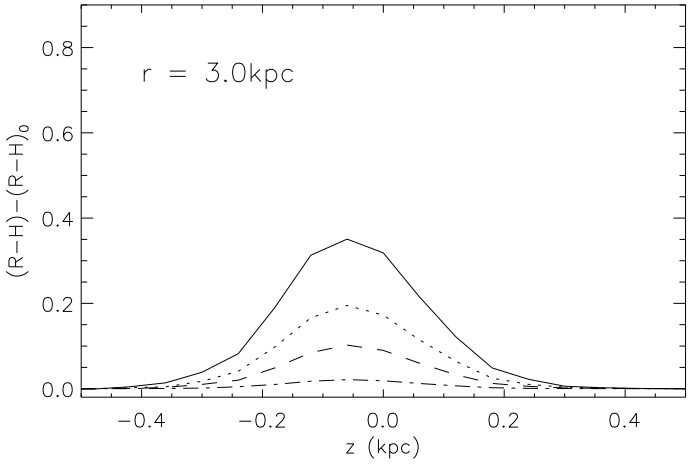
r = 3.0kpc
(R−H)−(R−H)0
z (kpc)

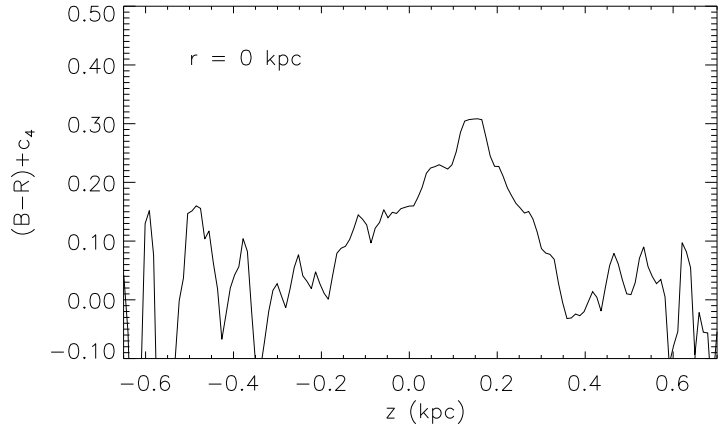
r = 0 kpc
(B−R)+c4
z (kpc)
0.50
0.40
0.30
0.20
0.10
0.00
−0.10
−0.6
−0.4
−0.2
0.0
0.2
0.4
0.6

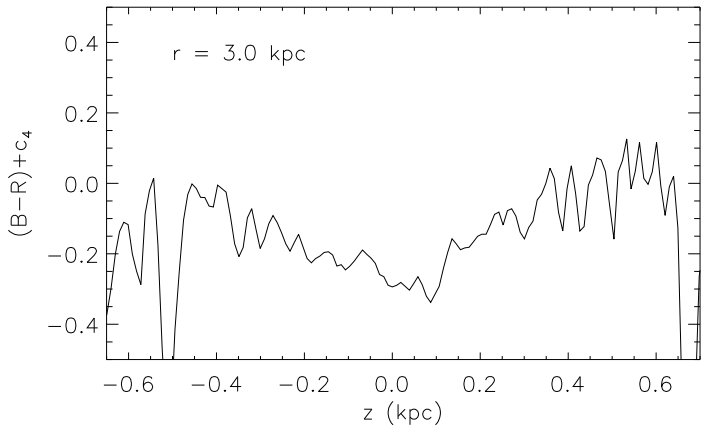
r = 3.0 kpc
(B−R)+c4
z (kpc)
0.4
0.2
0.0
−0.2
−0.4
−0.6
−0.4
−0.2
0.0
0.2
0.4
0.6

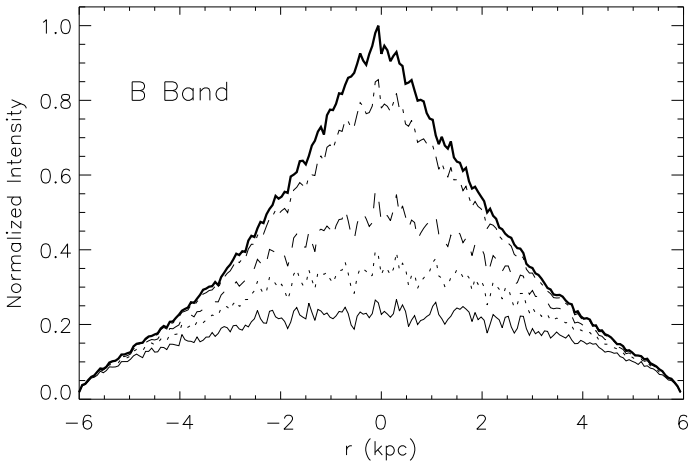
B Band
Normalized Intensity
r (kpc)
1.0
0.8
0.6
0.4
0.2
0.0
−6
−4
−2
0
2
4
6

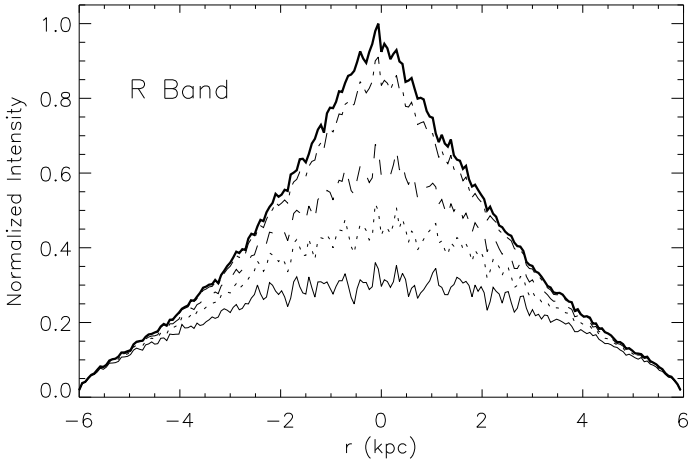
R Band
Normalized Intensity
r (kpc)
1.0
0.8
0.6
0.4
0.2
0.0
−6
−4
−2
0
2
4
6

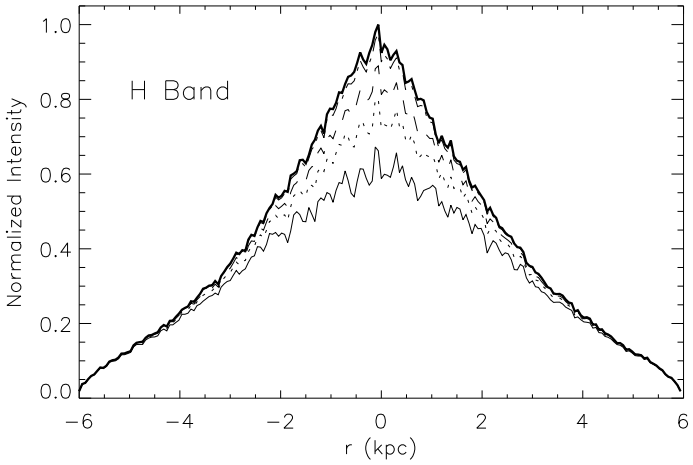
H Band
Normalized Intensity
r (kpc)
1.0
0.8
0.6
0.4
0.2
0.0
−6
−4
−2
0
2
4
6

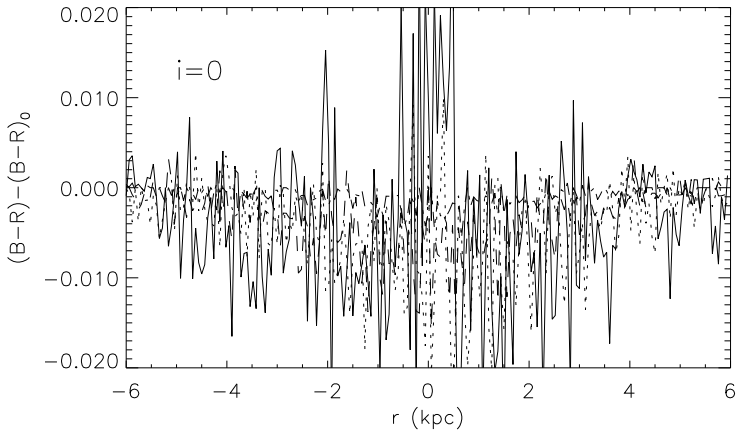
i=0
(B−R)−(B−R)$_0$
r (kpc)

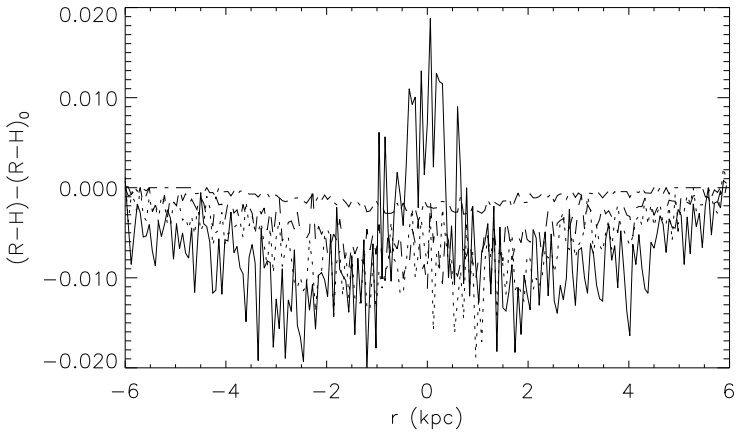
(R−H)−(R−H)$_0$
r (kpc)

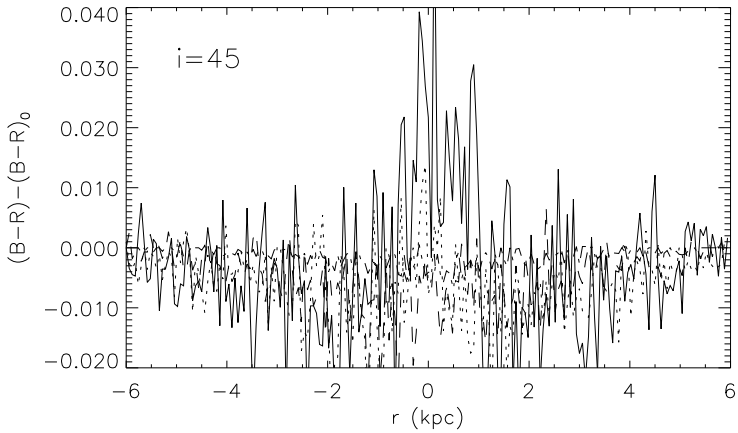
i=45
(B−R)−(B−R)$_0$
r (kpc)

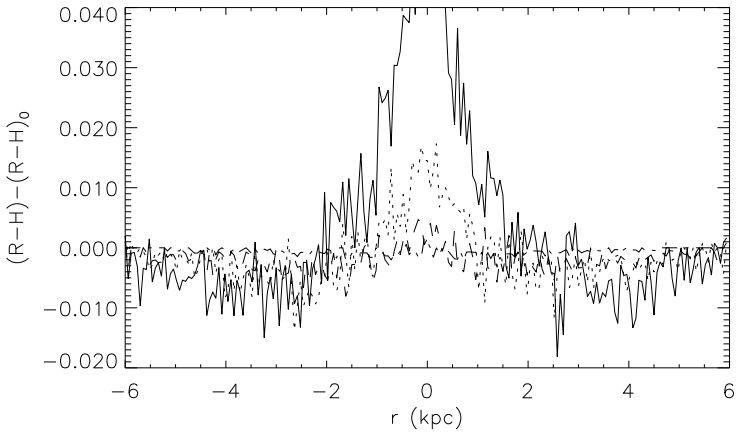
(R−H)−(R−H)$_0$
r (kpc)

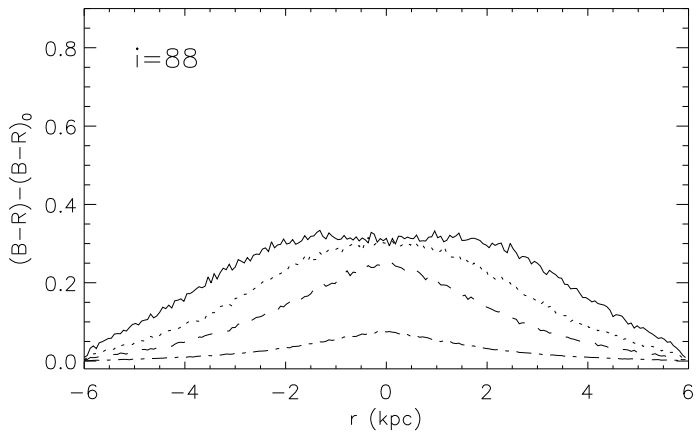
i=88
(B−R)−(B−R)$_0$
r (kpc)

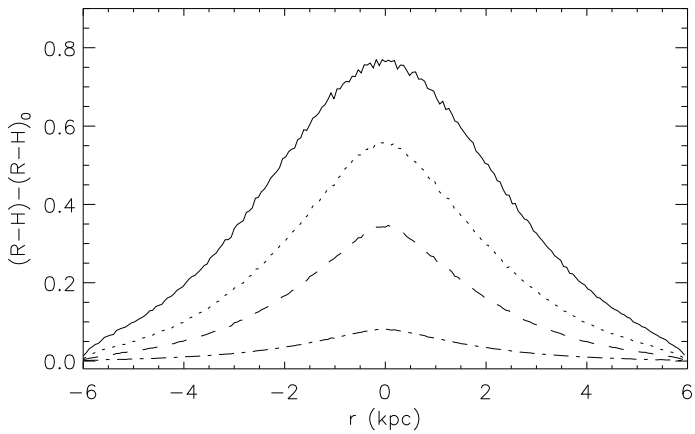
(R−H)−(R−H)$_0$
r (kpc)

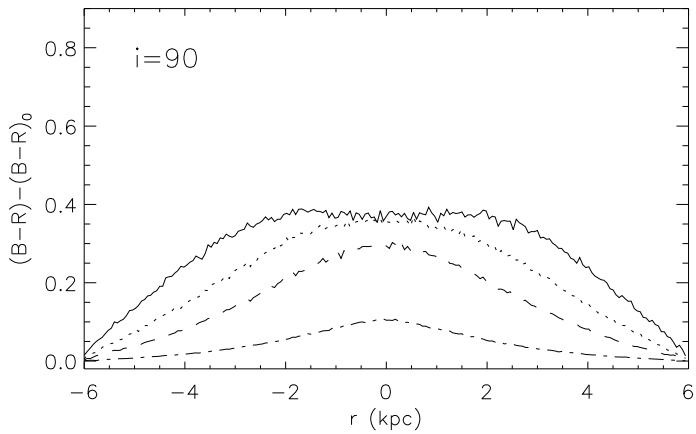
i=90
(B−R)−(B−R)$_0$
r (kpc)

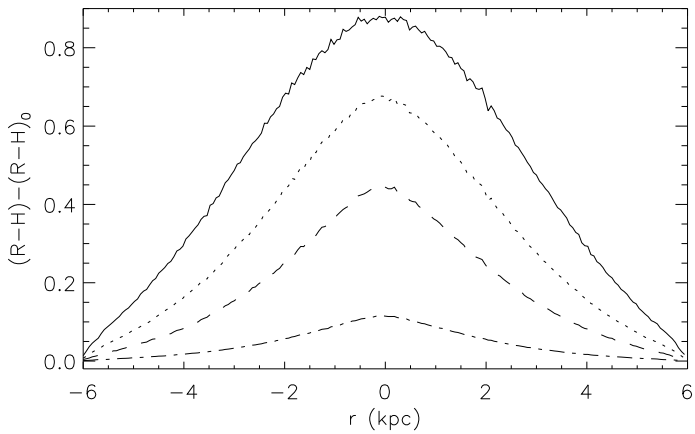
(R−H)−(R−H)$_0$
r (kpc)

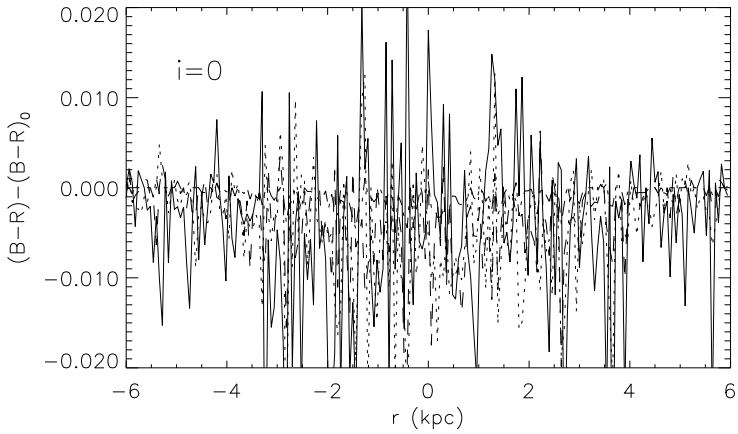
i=0
(B−R)−(B−R)0
r (kpc)

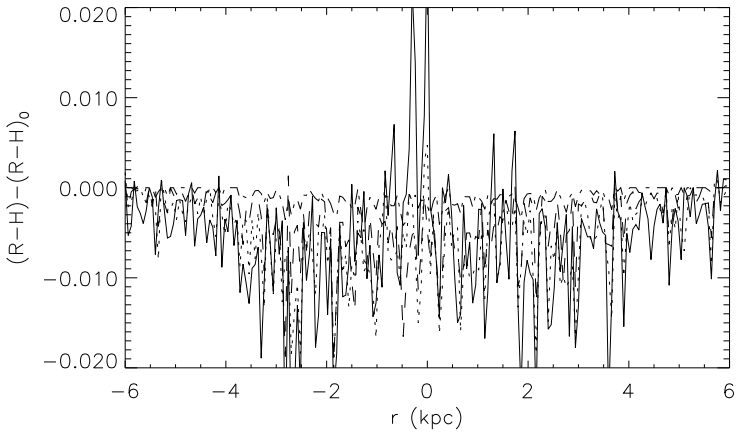
(R−H)−(R−H)0
r (kpc)

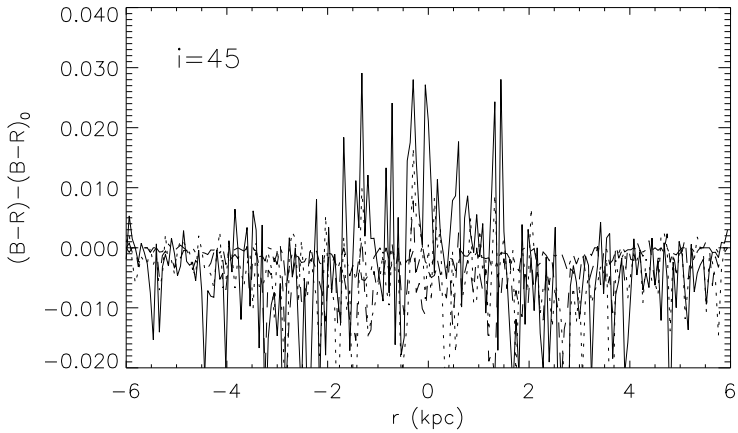
i=45
(B−R)−(B−R)0
r (kpc)

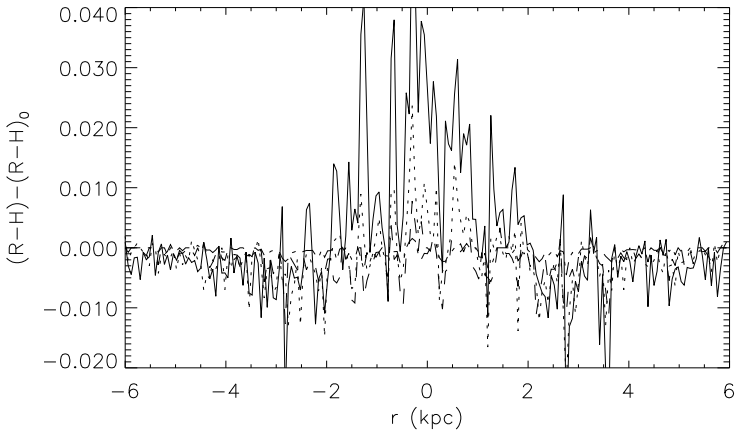
(R−H)−(R−H)0
r (kpc)

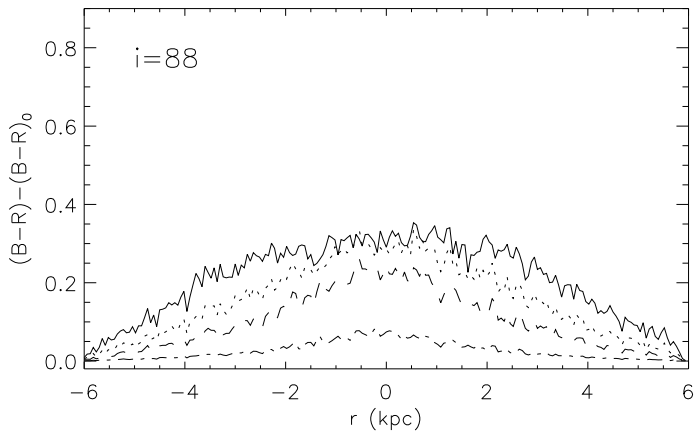
i=88
(B−R)−(B−R)0
r (kpc)

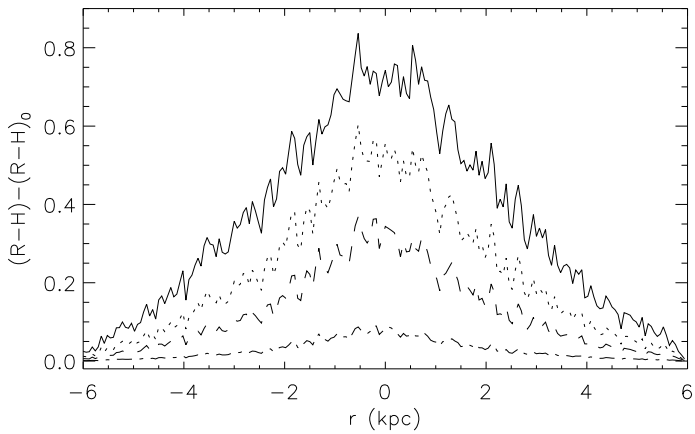
(R−H)−(R−H)0
r (kpc)

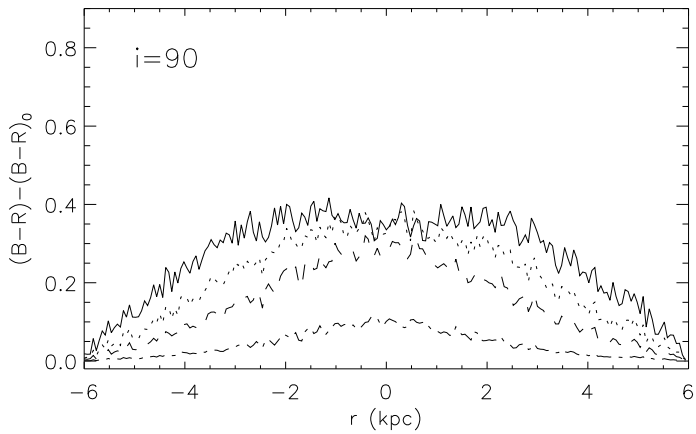
i=90
(B−R)−(B−R)0
r (kpc)

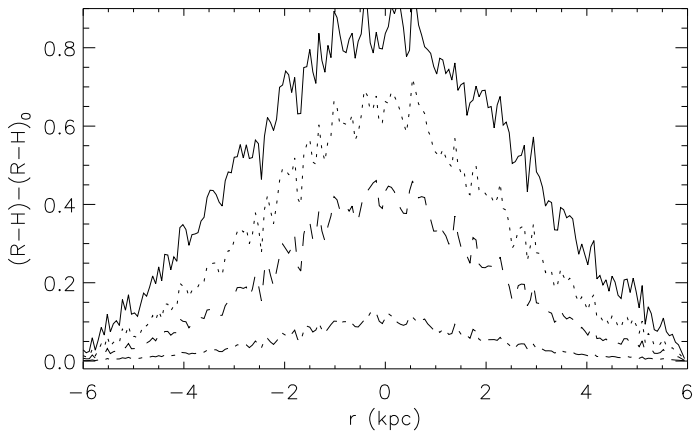
(R−H)−(R−H)0
r (kpc)

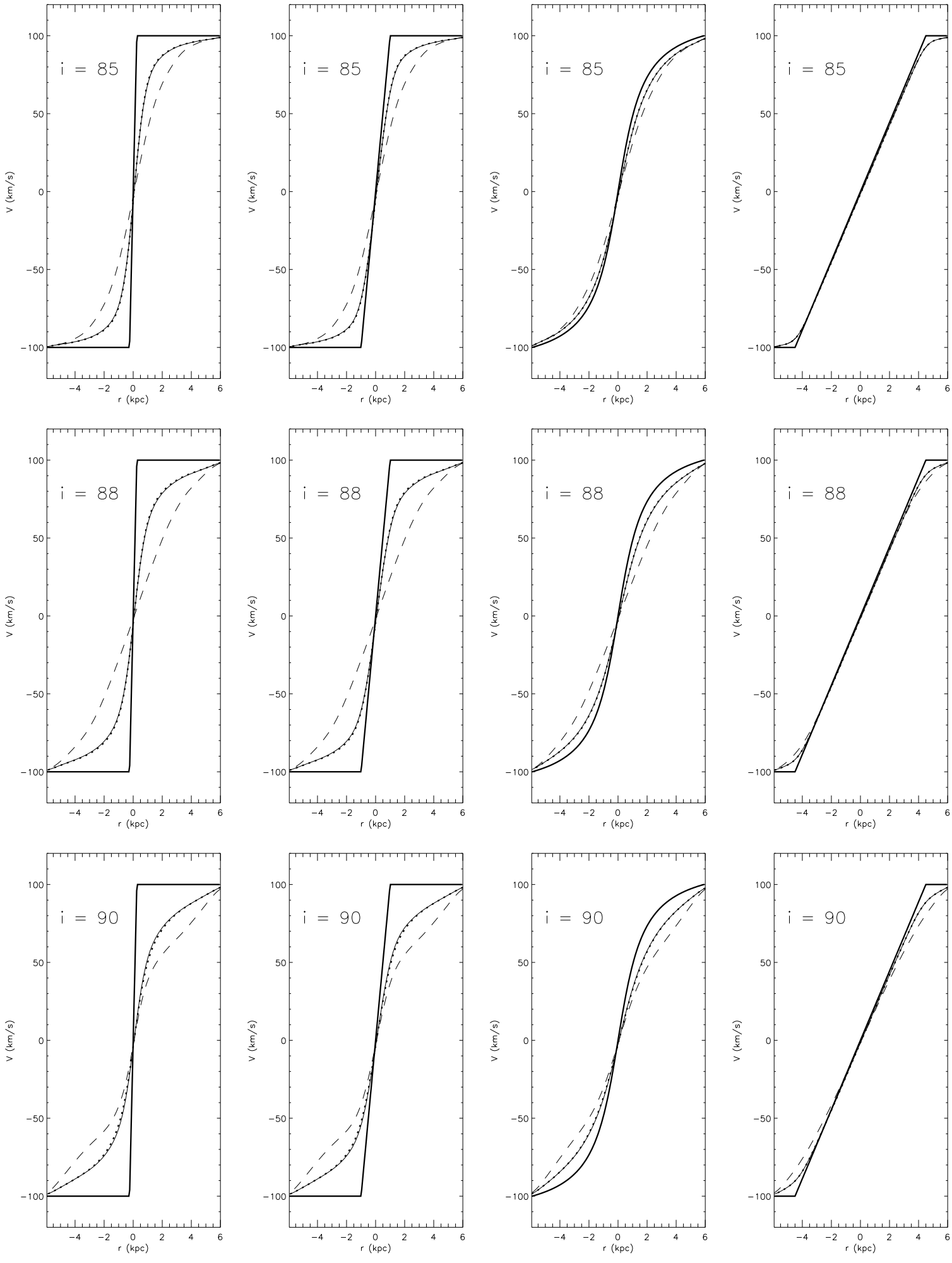
i = 85
i = 85
i = 85
i = 85
i = 88
i = 88
i = 88
i = 88
i = 90
i = 90
i = 90
i = 90
V (km/s)
r (kpc)
100
50
0
−50
−100
−4
−2
0
2
4
6

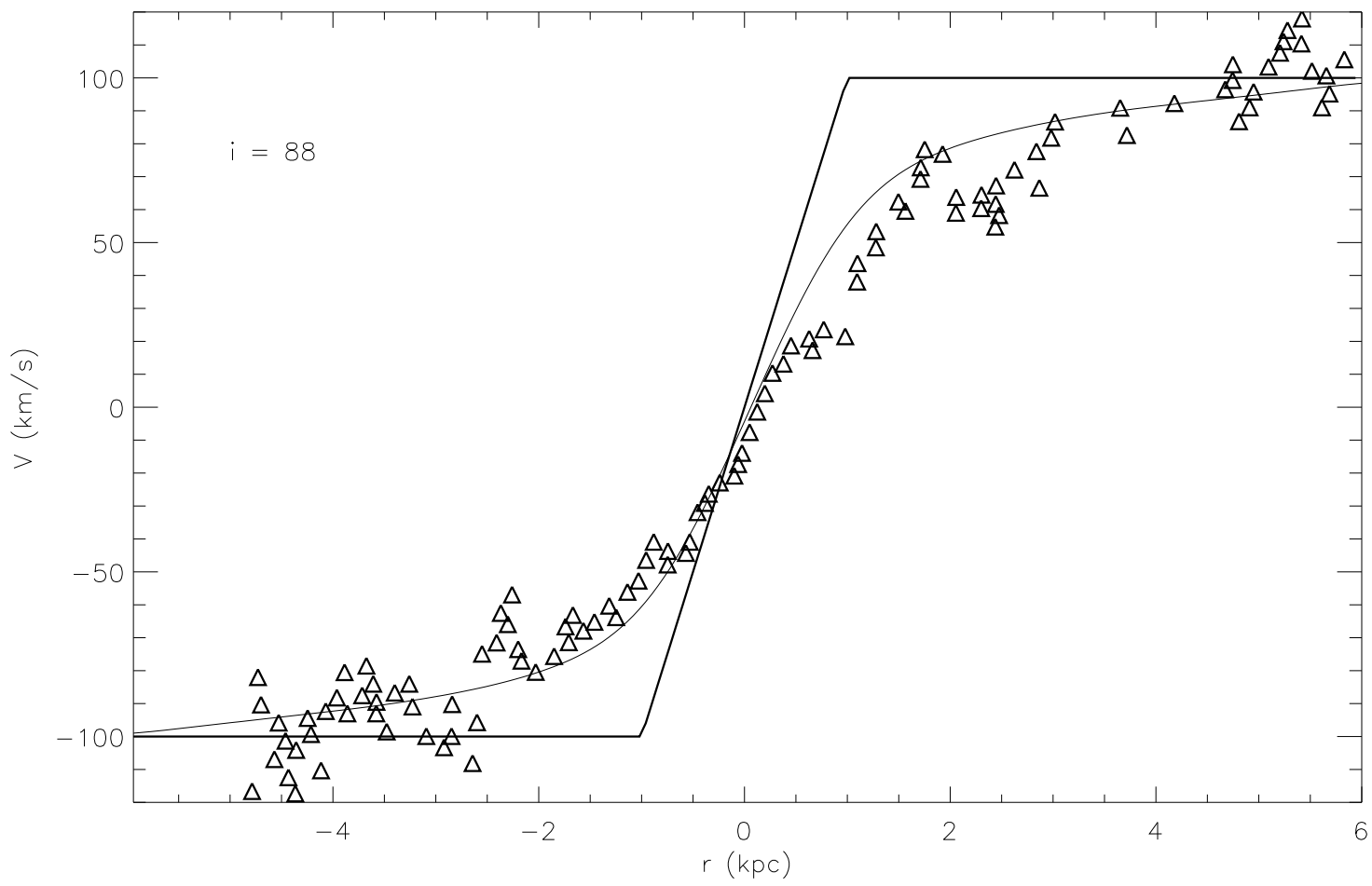
i = 88
V (km/s)
r (kpc)
100
50
0
−50
−100
−4
−2
0
2
4
6

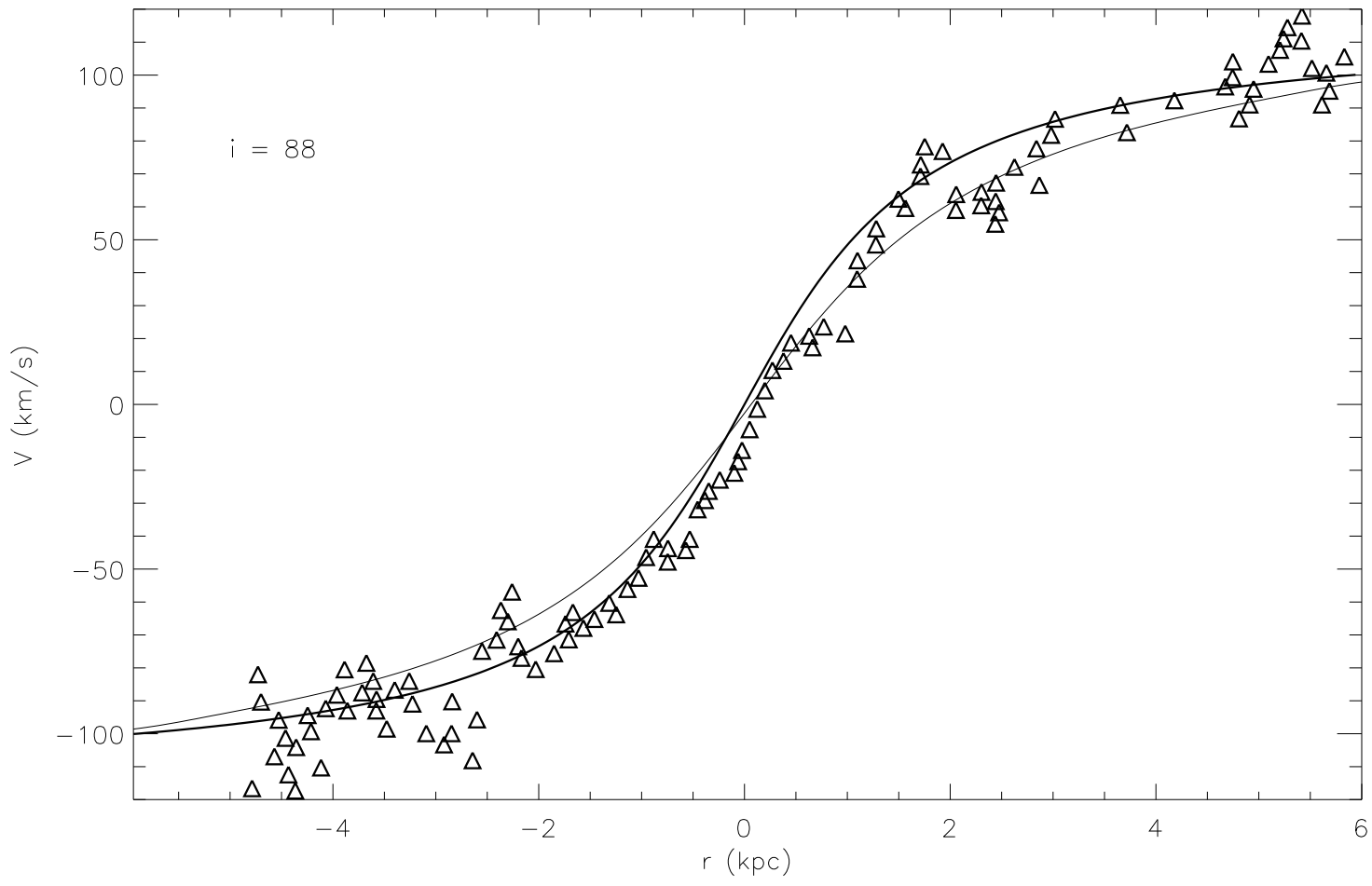
i = 88
V (km/s)
r (kpc)
100
50
0
−50
−100
−4
−2
0
2
4
6

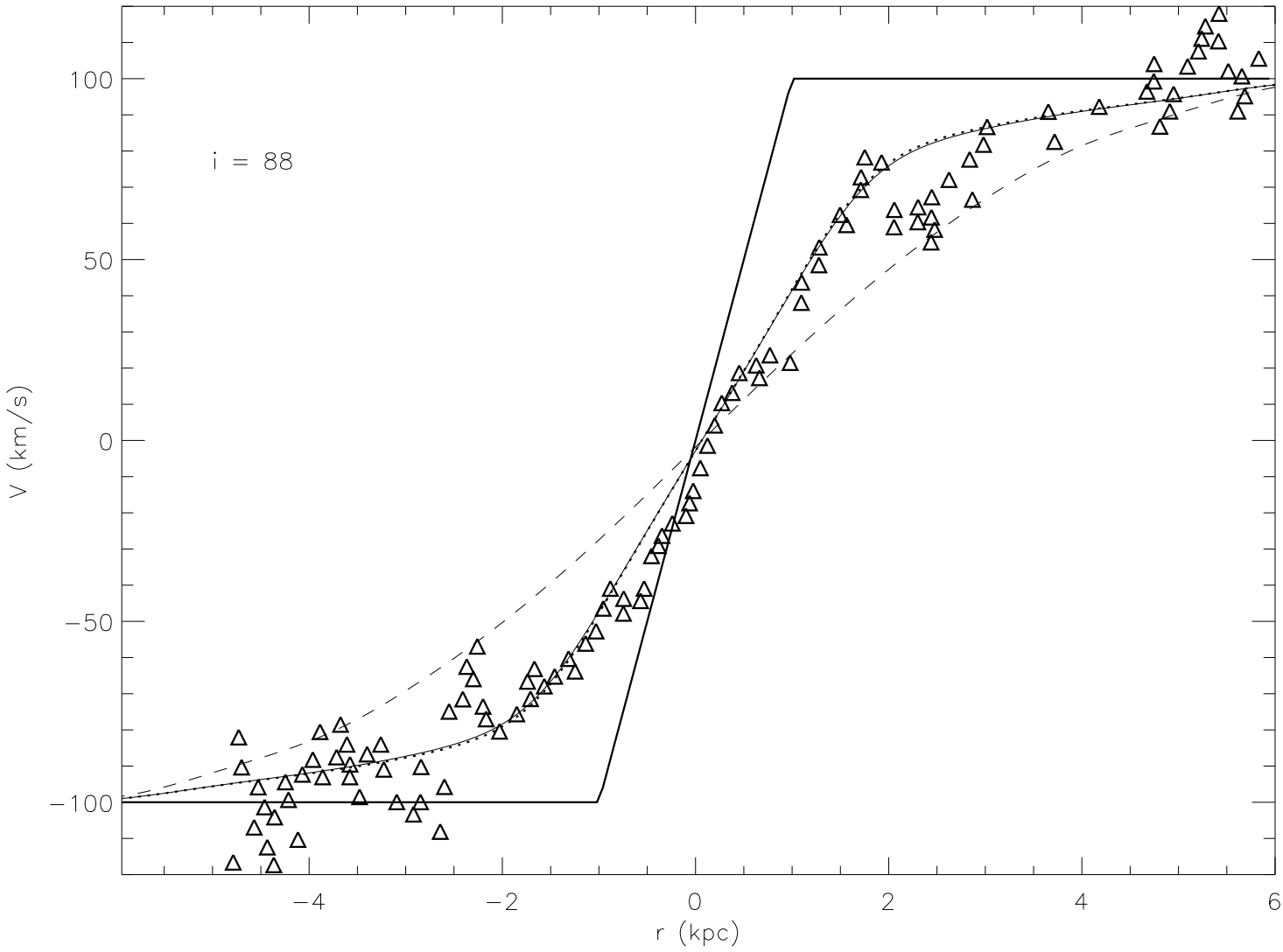
i = 88
100
50
0
−50
−100
V (km/s)
−4
−2
0
2
4
6
r (kpc)

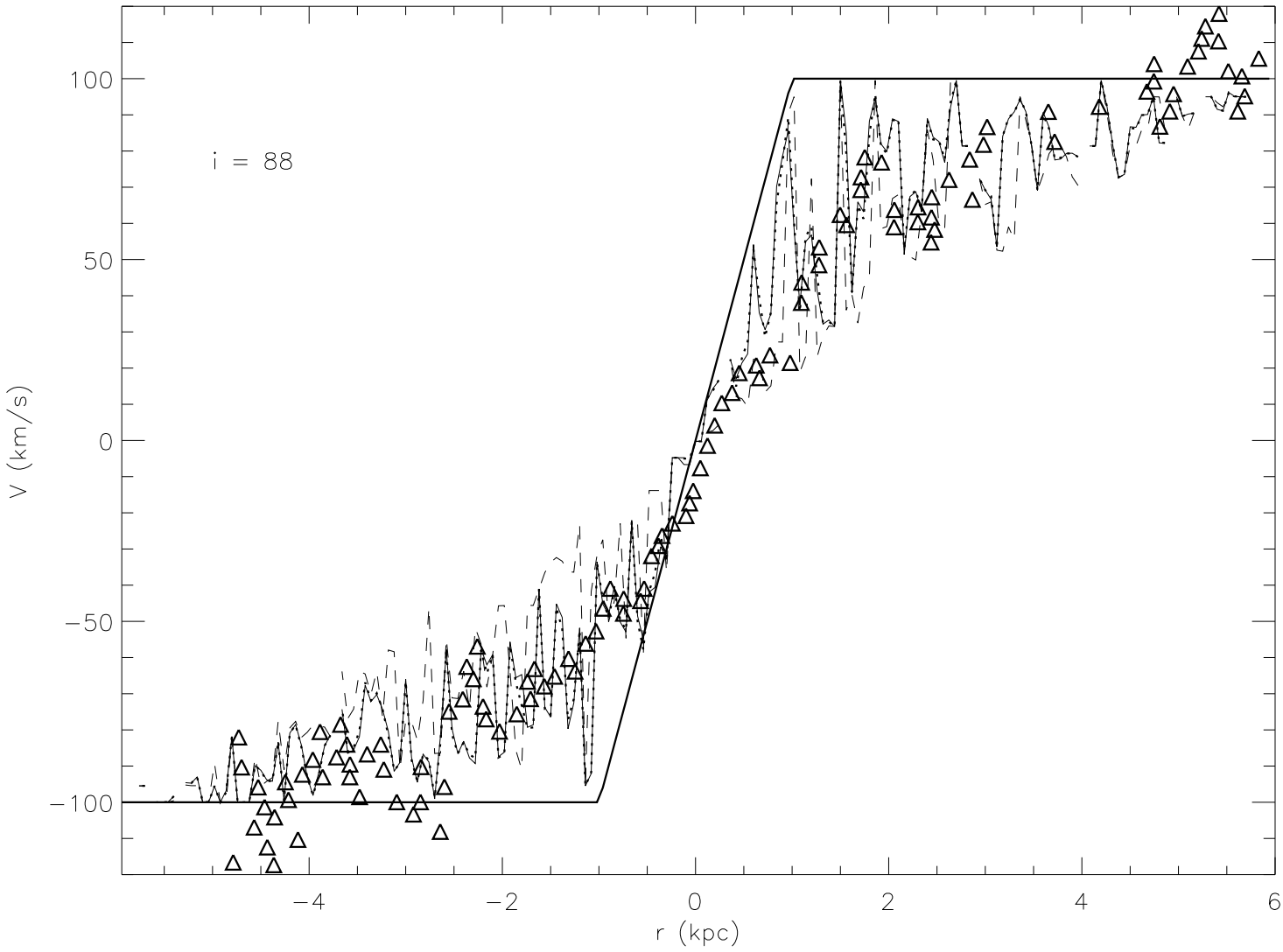
i = 88
100
50
0
−50
−100
V (km/s)
−4
−2
0
2
4
6
r (kpc)

Draft version February 1, 2008
Preprint typeset using LaTeX style emulateapj

arXiv:astro-ph/0010033v1 2 Oct 2000

MODELLING THE INTERSTELLAR MEDIUM OF LOW SURFACE BRIGHTNESS GALAXIES: CONSTRAINING INTERNAL EXTINCTION, DISK COLOR GRADIENTS, AND INTRINSIC ROTATION CURVE SHAPES

L. D. Matthews[1]
Kenneth Wood[2]

Draft version February 1, 2008

ABSTRACT

We use a combination of three-dimensional Monte Carlo radiative transfer techniques and multi-wavelength ($BRHK$, Hα) imaging data to investigate the nature of the interstellar medium (ISM) in the edge-on, low surface brightness (LSB) galaxy UGC 7321. Using realistic models that incorporate multiple scattering effects and clumping of the stars and the interstellar material, we explore the distribution and opacity of the interstellar material (gas+dust), and its effects on the observed stellar disk luminosity profiles, color gradients, and rotation curve shape. We find that UGC 7321 contains a small but non-negligible dusty component to its ISM, yielding a B-band optical depth $\bar{\tau}_{e,B}$ $\sim$4.0 from disk edge to center. A significant fraction ($\sim 50 \pm 10\%$) of the interstellar material in the innermost regions of UGC 7321 appears to be contained in a clumpy medium, indicating that LSB galaxies can support a modest, multi-phase ISM structure. In spite of the clear presence of dust, we conclude that the large radial optical color gradients observed in UGC 7321 and other similar LSB spiral galaxies cannot be accounted for by dust and must result primarily from significant stellar population and/or metallicity gradients. We show that realistic optical depth effects will have little impact on the observed rotation curves of edge-on disk galaxies and cannot explain the linear, slowly rising rotation curves seen in some edge-on LSB spirals. Projection effects create a far larger uncertainty in recovering the true underlying rotation curve shape of galaxies viewed at inclinations $i \gtrsim 85°$.

Subject headings: galaxies: ISM—ISM: dust, extinction—radiative transfer—galaxies: spiral—galaxies: kinematics and dynamics—galaxies: individual (UGC 7321)

1. INTRODUCTION

1.1. *Background*

Low surface brightness (LSB) disk galaxies can be broadly defined as rotationally-dominated galaxies with extrapolated face-on central surface brightness at least $\sim$1 magnitude fainter than the canonical Freeman (1970) value of $\mu_{B,0}$ =21.65 mag arcsec^{-2}. Although LSB galaxies span the full range of Hubble types (e.g., Schombert *et al.* 1992), here we use the term primarily in reference to the latest type spirals (Scd-Sdm). Numerous observational studies have now shown that LSB galaxies are not "abnormal" objects, but rather are a common product of disk galaxy formation and evolution. More extensive summaries of the properties of LSB galaxies can be found in Bothun, Impey, & McGaugh (1997) and Impey & Bothun (1997) and references therein.

In spite of the vast body of multiwavelength observational data now accumulated on LSB galaxies, several aspects of these systems still remain enigmatic. One important example is the detailed nature of their interstellar medium (ISM). Although the bulk of LSB galaxies are known to be rich in neutral hydrogen gas (H I), they are generally presumed to be dust and molecule-poor systems. Numerous observations directly and indirectly support this picture, including: low metal abundances (e.g., McGaugh 1994; Rönnback & Bergvall 1995), low statistically inferred internal extinctions (e.g., Tully *et al.* 1998; Matthews, van Driel, & Gallagher 1998), strong similarities between optical and near-infrared (NIR) morphologies (Bergvall *et al.* 1999); undetectable CO fluxes (Schombert *et al.* 1990; Knezek 1993; de Blok & van der Hulst 1998; but see Matthews & Gao 2000), and the high transparency of their stellar disks (e.g., O'Neil *et al.* 1998; Matthews *et al.* 1999; Matthews, Gallagher, & van Driel 1999, hereafter MGvD99). Theoretical and numerical models also suggest that the low surface densities and low metallicities of LSB galaxies cannot support significant molecular gas fractions (e.g., Mihos, Spaans, & McGaugh 1999; Gerritsen & de Blok 1999). Nonetheless, since most presently known LSB galaxies are actively star-forming systems, having blue disk colors and at least modest amounts of Hα emission, it seems likely that at least some molecular material must be present in these systems.

Even if dust and molecular gas contents in LSB galaxies are typically small, extinction and reddening due to interstellar material may still have a non-negligible impact on the observed properties of these galaxies, and molecular gas could still be an important constituent of the ISM (e.g., Spaans 1999). For example, estimates of dust reddening, even if small, are needed to correctly interpret the stellar populations inferred from broad-band colors and spectroscopic measurements (e.g., Bell *et al.* 2000). It has

[1]National Radio Astronomy Observatory, 520 Edgemont Road, Charlottesville, VA 22903 USA, Electronic mail: lmatthew@nrao.edu
[2]Smithsonian Astrophysical Observatory, 60 Garden Street, Cambridge, MA 02138 USA, Electronic mail: kenny@claymore.harvard.edu

been found that many of the lowest-luminosity LSB galaxies deviate from the standard optical Tully-Fisher relation in the sense that they rotate faster than predicted for their luminosities (e.g., Matthews, van Driel, & Gallagher 1998; Stil 1999; McGaugh *et al.* 2000), while more luminous LSB galaxies seem to follow the same Tully-Fisher relation as higher surface brightness galaxies (e.g., Zwaan *et al.* 1995; Sprayberry *et al.* 1995). This appears to have important implications for galaxy formation models (e.g., van den Bosch 2000) and for establishing the possible existence of a "baryonic" Tully-Fisher relation (e.g., Matthews, van Driel, & Gallagher 1998; McGaugh *et al.* 2000); however, the internal extinction corrections appropriate for the LSB galaxies used in these analyses remains a point of contention (e.g., Han 1992; Rhee 1996; Matthews, van Driel, & Gallagher 1998; Pierni 1999). Lastly, rotation curves of LSB galaxies offer hope to furthering our insight into the nature of dark matter in galaxies (e.g., de Blok & McGaugh 1997; McGaugh & de Blok 1998; Kravtsov *et al.* 1998; Swaters, Madore, & Trewhella 2000). Accurately interpreting high resolution optical rotation curve data, which can play a crucial part in such analyses, requires an assessment of the role of internal extinction in these systems (see Section **??**). In short, a more extensive and quantitative knowledge of the total amounts and distribution of dust and other molecular material in LSB disks is overall vital to better understanding the global properties as well as the star-forming and evolutionary histories of these systems.

To date, few attempts have been made to model the dust in individual LSB galaxies in a sophisticated manner. One difficulty is that these objects tend to be very weak far-infrared and sub-millimeter sources (e.g., Hoeppe *et al.* 1994; Pickering & van der Hulst 1999; Bell *et al.* 2000), hence direct observations of re-emitted thermal radiation from their dust are lacking. Observing the dust in absorption at optical and near-infrared wavelengths can also be problematic, since for LSB systems viewed at moderate or low inclinations, the signatures of dust can be difficult to infer against the patchy and diffuse background light of the stellar disk. The data necessary to test dust models are therefore sparse. For these reasons, *edge-on* examples of LSB galaxies are particularly valuable.

Because the viewing geometries of edge-on LSB galaxies provide maximal path length through the disks, such systems furnish us with the unique opportunity to directly observe the vertical and radial extent of the dust distribution, as well as any associated dust-induced vertical and radial color gradients. With the aid of 3D radiative transfer models, it becomes possible to constrain the amount and distribution of dust and quantify its effects on the observed properties of the galaxy, including: total internal extinction, effects on observed color gradients, and effects on the disk rotation curve. Properties of the disk viewed at other arbitrary inclinations can also be predicted. Such techniques have been used to explore the effects of dust in more luminous, high surface brightness galaxies seen edge-on (e.g., Kylafis & Bahcall 1987; Kuchinski & Terndrup 1996; Kuchinski *et al.* 1998; Trewhella, Madore, & Kuchinski 1999; Xilouris *et al.* 1997,1998,1999). Here we present one of the first applications of full 3-D Monte Carlo radiative transfer techniques to studying systems at the low optical depth regime of LSB galaxy disks.

1.2. *UGC 7321: A "Superthin" LSB Galaxy*

UGC 7321 is a nearby example of an Sd spiral galaxy with an extraordinarily thin, highly flattened and diffuse stellar disk with no obvious bulge component (MGvD99; Matthews 2000). MGvD99 showed that this "superthin" galaxy is actually an example of an LSB spiral galaxy seen near edge-on ($i \approx 88°$). MGvD99 estimated that after correction for projection and internal extinction, UGC 7321 would have a B-band central disk surface brightness $\mu_{B,i}(0)$ ∼23.6 mag arcsec^{-2}.

Although the *observed* surface brightness of UGC 7321 is enhanced through projection, several lines of evidence clearly indicate this is an intrinsically LSB galaxy, independent of internal extinction corrections. These include: the extreme transparency of its disk (e.g., several background galaxies are clearly visible directly through it; MGvD99); the small stellar scale height and very low estimated stellar velocity dispersion (implying a very low disk surface density; Matthews 2000); low emission line intensity ratios (Goad & Roberts 1981); weak far-infrared and radio continuum emission (see below); and a rather high M_{HI}/L_B ratio (1.1 in solar units).

UGC 7321 is an ideal LSB galaxy for detailed modelling since it is nearby ($D \approx 10^{+3}_{-3}$ Mpc; Gallagher *et al.* 2000) and well-resolved. Some key properties of UGC 7321 are summarized in Table 1. Although UGC 7321 is physically smaller, less massive, and less luminous than most other well-studied edge-on spirals, UGC 7321 appears to be a prototypical example a relatively common class of late-type LSB galaxies seen on edge (see also Goad & Roberts 1981; Karachentsev, Karachentseva, & Parnovsky 1993; Bergvall & Rönnback 1995; Dalcanton & Schectman 1996; Gerritsen & de Blok 1999; Matthews & van Driel 2000). Possible face-on analogs of UGC 7321 might be such systems as NGC 4395 (see Sandage & Bedke 1994) or ESO 305-009 (see Matthews & Gallagher 1997).

1.2.1. *The Data*

Much of the primary observational data we use for our present analysis were described in MGvD99; these include near-infrared (NIR) H-band and optical (B- & R-band) imaging data, and narrow-band Hα imaging of UGC 7321. In addition, we supplement these data with observations from several additional sources. *Hubble Space Telescope* (*HST*) Wide Field and Planetary Camera 2 $F702W$ and $F814W$ (R- and I-band equivalent) imaging observations of the inner disk regions of UGC 7321 (Figure 1) are an important component of our study and will be discussed further in Gallagher *et al.* (2000). We also used the optical longslit rotation curve data of Goad & Roberts (1981), and NIR H and K_s images of UGC 7321 obtained from the Two Micron All Sky Survey (2MASS) database (http://sirtf.jpl.nasa.gov/2mass/).

1.2.2. *Color Gradients in UGC 7321*

One particularly intriguing finding of MGvD99 is that UGC 7321 exhibits quite strong radial color gradients: $\Delta(B-R)$ ∼1.0 magnitude (before correcting for internal reddening), with the outer disk regions being considerably bluer than the galaxy center (Figure 2). These authors interpreted this as evidence of significant stellar age gradients as a function of radius in the disk, and suggested

that this is a galaxy that is likely to have evolved relatively slowly, from the inside out. Large radial color gradients [$\Delta(B-R) \gtrsim 0.5$] were also reported for a sample of 3 additional superthin galaxies by Matthews, Gallagher, & van Driel (2000). The strength of the observed color gradients in UGC 7321 may also indicate that viscous evolution has been minimal in this disk (cf. Firmani, Hernández, & Gallagher 1996), leading MGvD99 to postulate that galaxies like UGC 7321 may be some of the most pristine star-forming disks in the nearby universe, and hence ideal systems in which to explore disk evolutionary processes.

MGvD99 also reported significant *vertical* color gradients in the UGC 7321 disk (as large as $\Delta(B-R) \sim 0.45$, with the colors reddening as a function of increasing z height). Such gradients are predicted to occur in galaxy disks as a result of dynamical heating processes (e.g., Just, Fuchs, & Wielen 1996), but in practice they are difficult to observe and interpret in most edge-on galaxies due to the effects of seeing, contamination from bulge light, and particularly due to contamination from dust. Thus relatively few empirical constraints exist for present models of vertical disk heating.

A critical assumption in interpreting the physical significance of the large color gradients observed in the UGC 7321 disk, as well as the significant gradients observed in the disks of other less inclined LSB spirals (e.g., de Blok, van der Hulst, & Bothun 1995; Bell *et al.* 2000) is that reddening due to dust is small. For example, in a sample of "normal" edge-on spirals, de Grijs (1998) argued that to within observational errors, the observed color gradients and scale length differences in different wavebands could be explained solely from dust.

Based on *HST* imaging observations, Matthews (1998) and Gallagher *et al.* (2000) have shown that although UGC 7321, as well as another nearby, edge-on LSB system UGC 711 lack the quintessential dust lanes seen in brighter edge-on spirals (cf. Howk & Savage 1999), they are not dust-free. Nonetheless, using a simple foreground screen model, MGvD99 suggested that in the case of UGC 7321, dust reddening could not explain more than $\sim$0.2 magnitudes of the observed $B-R$ color gradient. Using both foreground screen and Triplex dust models (see Disney, Davies, & Phillipps 1989), Bell *et al.* (2000) argued that the amount of dust reddening needed to produce the observed color gradients in their sample of less inclined LSB galaxies was also too large to be consistent with observations.

To obtain a first estimate of the role of dust in UGC 7321, MGvD99 employed a simple foreground screen model. These authors sought not to derive a realistic dust model for UGC 7321, but rather to test the possibility that a significant fraction of the observed color gradient in UGC 7321 could be caused by dust. To put an upper limit on the dust-induced color gradient, these authors assumed that the galaxy was effectively optically thin in H, and that the entire observed $R-H$ radial color gradient could be due to dust.

A reanalysis of the $R-H$ color profile of UGC 7321 (Figure 3), actually shows a significantly larger color gradient ($\sim 0.9 \pm 0.1$ mag) than that reported by MGvD99. This difference was traced to an error by MGvD99 in extracting the H-band radial axis profile. However, because MGvD99 were extremely conservative in their attribution of the full $R-H$ color gradient to possible dust reddening, as we further demonstrate here, the validity of their final conclusions remains unaffected.

Although the arguments presented by MGvD99 and Bell *et al.* (2000) regarding the dust reddening in their sample LSB galaxies are expected to be for the most part robust, they nonetheless relied on simplifying assumptions, including the use of smooth, idealized dust geometries and the neglect of scattering effects. And because the color gradients observed in UGC 7321 and some other LSB galaxies are often found to be large compared with those typical in most normal surface brightness spiral galaxies (cf. de Jong 1996), it is important to establish (1) whether galaxies like it are in fact a genre of nearby disks with some of the largest intrinsic color gradients, (2) whether these are pathological LSBs that contain more dust than average, and (3) whether our knowledge of the dust in typical LSB galaxies is somehow incomplete. Detailed studies of individual galaxies rather than statistical studies are needed to address these questions. If the large observed color gradients are intrinsic (i.e., due to true stellar population and/or metallicity gradients) rather than a result of dust reddening, this is important not only for understanding the evolution and stellar contents of these and other LSB disks, but also because such gradients may imply non-negligible changes in the stellar mass-to-light ratio ($\Upsilon_\star$) of disks as a function of radius. Such trends could have an important consequence for mass-modelling of LSB galaxies (i.e., for determining their dark matter halo parameters from rotation curves; e.g., Kent 1986) and understanding the underlying physics behind the Tully-Fisher relation (cf. Matthews, van Driel, & Gallagher 1998; Stil 1999; McGaugh *et al.* 2000). It is of interest therefore to derive sophisticated, realistic dust models of UGC 7321 as a first test case.

We note that an advantage of studying color gradients in edge-on or near edge-on disks is that due to the higher projected surface brightnesses of the outer disk compared to a face-on system, we can better observe the faintest (and perhaps least evolved) outer disk regions. The trade-offs are of course the uncertain effects of dust toward the central disk regions, as well as the possible superposition of many different stellar populations along a given line of sight. This makes the use of full three-dimensional (3D) models critical for unravelling the effects of dust on the observed colors and inferred stellar population distributions. This is the approach we utilize in the present work.

1.3. *The Present Study*

The fundamental questions this paper seeks to address are:

- What is the integrated optical depth of the dusty medium in UGC 7321, and what are its total mass and distribution?
- What internal extinction corrections are appropriate for edge-on LSB galaxies?
- How much of the observed color gradients in UGC 7321 and other similar galaxies can be attributed to dust?
- What are the predicted dust-induced color gradients

for analogous LSB disks seen at alternate viewing angles?

- What is the impact of optical depth effects on the shape of optically-derived rotation curves of LSB galaxies observed near edge-on?

To answer these questions we use a suite of high resolution, 3D Monte Carlo radiation transfer codes that simulate scattered light images in multiple wavebands and also can be used to model the effects of dust on optical rotation curves. As described below, our Monte Carlo radiation transfer code has recently been modified (see Wood & Reynolds 1999 and Section 2.1) to enable the efficient simulation of 3D, optically thin systems, thus making it ideal for our present study of LSB galaxies. In doing this we also lay the groundwork for future studies of the nature of dust in other LSB galaxies. Much of the general framework required for realistically modelling the effects of dust in galaxies has been discussed extensively by others (e.g., Kylafis & Bahcall 1987; Bosma *et al.* 1992; Xilouris *et al.* 1997,1998,1999), including the application of Monte Carlo methods to galactic environments (e.g., de Jong 1996; Witt & Gordon 1996,2000; Kuchinski *et al.* 1998; Bianchi, Ferrara, & Giovanardi 1996; Bianchi *et al.* 2000). We do not attempt to repeat the detailed findings of these works here, but rather apply our codes to explore specific questions relating to LSB galaxies. In particular, in this paper we focus on using our Monte Carlo models to reproduce the observed properties of the edge-on LSB galaxy UGC 7321 and to predict the role dust may play on the observed properties of similar LSB galaxies viewed over a range of inclinations.

2. THE MODELS

The ingredients needed for our models of the dusty ISM of UGC 7321 are a 3D Monte Carlo radiation transfer code, measurements of dust and stellar distributions within the galaxy, and a characterization of the galactic velocity field. The outputs of a Monte Carlo simulation are scattered light images (Sect. 3.1 & 3.2.1) and rotation curves that include the effects of internal extinction (Sect. **??**). We now describe the model inputs.

2.1. *Radiation Transfer Treatment*

In the present investigation, we perform radiation transfer calculations with a 3D Monte Carlo scattering code that tracks photon energy packets as they are scattered and absorbed in a model galaxy. The code is based on that described by Code & Whitney (1995) and has been modified from the version used for the smooth density and emissivity models of Wood (1997) and Wood & Jones (1997) to enable us to study fully three dimensional systems (Wood & Reynolds 1999). We construct the galactic density, emissivity, and velocity structure on a 3D linear Cartesian grid, and in the Monte Carlo radiation transfer, we now incorporate forced first scattering (Witt 1977) and a peeling off procedure (Yusef-Zadeh, Morris, & White 1984). This enables us to very efficiently generate images and rotation curves for the 3D, optically thin systems we are investigating (see also Wood & Reynolds 1999). Unlike more simplistic dust treatments, our code models both absorption and multiple scattering of photons; both are necessary for accurately determining the total amount of dust in a galaxy (e.g., Witt, Oliveri, & Schild 1990; Block *et al.* 1994) and for predicting its observational manifestations.

2.2. *Stellar Emissivity and Dust Distributions*

In Monte Carlo simulations of the transfer of starlight through galaxies, the stellar sources are often represented by a smooth spatial distribution (e.g., Wood & Jones 1997; Ferrara *et al.* 1996, 1999; Bianchi, Ferrara, & Giovanardi 1996) rather than by individual point sources (but see recent work by Cole, Wood, & Nordsieck 1999; Wood & Reynolds 1999). However, because spiral disks seldom are observed to have completely smooth, uniform disks at optical and NIR wavelengths, here we also consider the case of starlight with an additional non-uniform component superposed on a smooth background (see below).

In a purely smooth case, for a galaxy disk that is exponential in the radial and vertical directions, the stellar emissivity can be expressed as

$$L(r,z) = L_{\lambda,0}\exp\left(-\frac{r}{h_r} - \frac{|z|}{h_z}\right) \tag{1}$$

where r and z are the usual cylindrical coordinates, $L_{\lambda,0}$ is the central disk surface density at a given waveband, and h_r and h_z are the scale length and scale height, respectively, of the stars. If a bulge is present, an additional term will be required in the emissivity distribution.

A smooth density distribution of interstellar material (i.e., gas+dust), also assumed to be exponential in both the radial and vertical directions, can be expressed as

$$\rho(r,z) = \rho_0\exp\left(-\frac{r}{h_{r,d}} - \frac{|z|}{h_{z,d}}\right) \tag{2}$$

where ρ_0 is the density (in g cm^{-3}) at the galactic center, and $h_{r,d}$ and $h_{z,d}$ are the scale length and scale height, respectively, of the dust. We then define an edge-on optical depth in the B-band, $\tau_{e,B}$, measured from the disk edge to the disk center, as

$$\tau_{e,B} = \int \rho(r,0)\kappa_B \mathrm{d}r \approx \rho_0\kappa_B h_{r,d} \tag{3}$$

where the absorption coefficient κ_B characterizes the opacity of the dust+gas mixture (see Sect. 2.3).

Because the ISM in real galaxies is not purely smooth, several recent papers have examined the dust scattering of radiation in a two-phase medium, with emphasis on the penetration and escape of stellar radiation from clumpy environments (Boissé 1990; Witt & Gordon 1996, 2000; Bianchi *et al.* 2000). In all of these studies, clumping allowed photons to penetrate to greater depths than in a smooth medium, and the escape of radiation becomes enhanced relative to the case where the same gas and dust mass was distributed smoothly. The ability of Monte Carlo techniques to straightforwardly incorporate these effects into models helps to make this technique particularly powerful, hence we also explore the role of clumping in our models in the present study.

For our study of the disk of UGC 7321 we adopt the prescription for a two-phase interstellar medium from Witt & Gordon (1996). Here the medium consists of a smooth

component and a clumpy medium. This medium is characterized in terms of two parameters, namely the volume filling factor of dense clumps, ff, and the density contrast between the clump and interclump medium, C. C in effect determines the total amount of mass contained in the smooth versus the clumped ISM component. We emphasize that in the work that follows, such models generally contain *both* a clumpy and a smoothly distributed ISM component; however, we hereafter refer to these simply as "clumpy" models.

We transform our smooth density distribution from Eq. 2 into a clumpy one by looping through our 3D grid and applying the following algorithm in each grid cell

$$n_{\rm clumpy} = \begin{cases} n_{\rm smooth}/[ff + (1-ff)/C], & \text{if } \xi < ff; \\ n_{\rm smooth}/[ff(C-1)+1], & \text{otherwise.} \end{cases} \quad (4)$$

where ξ is a uniform random deviate in the range (0,1). This algorithm assures that *on average* the total disk mass is the same for a clumpy model as in a purely smooth model of a given optical depth, and that the ensemble average of the clumpy distribution follows the same spatial profile as the smooth gas does. In this approach the smallest clump is a single cell in our density grid (Sect. 2.4).

We have also applied the algorithm given by Eq. 4 to generate a clumpy *emissivity* distribution, as could result, for example, from clusters of young stars superposed on a smoother underlying disk of older stars. We discuss our choices for ff and for C for both the stellar and gas+dust distributions further below.

2.3. *Dust Opacity and Scattering Properties*

We assume that the dust plus gas in our model galaxies is represented by a Kim, Martin, & Hendry (1994) gas+dust mixture. The Kim *et al.* models are an extension of the models of Mathis, Rumpl, & Nordsieck (1977) to include a larger distribution of grain sizes, yielding a higher (and more realistic) estimate of the NIR opacity. The wavelength dependent parameters defining this model are the total opacity, κ_λ, scattering albedo, a_λ, and phase function asymmetry parameter, g_λ. The scattering phase function is approximated by the Heyney-Greenstein phase function (Heyney & Greenstein 1941). In Table 2 we tabulate the adopted dust parameters for our simulations.

The total amount of dust in all of our models is characterized by the optical depth parameter $\tau_{e,\lambda}$ (Eq. 3), which is the optical depth of the model galaxy to a photon of wavelength λ as it travels from the galaxy center through the disk midplane to the observer. The corresponding optical depth in the polar direction, through the galactic center, is

$$\tau_{p,\lambda} = (h_{z,d}/h_{r,d})\tau_{e,\lambda}.$$

The Kim *et al.* (1994) gas+dust models that we employ are formulated to specifically represent *Galactic* grain properties, and assumes a Galactic gas-to-dust ratio of 140. Because the gaseous component of this ISM mixture contributes a negligibly small fraction of the total opacity, this assumption of a Galactic gas-to-dust ratio will have no effect on extinction or reddening effects derived from our models. The actual gas-to-dust ratio appropriate for UGC 7321 is discussed further in Sect. 3.6.1.

Evidence suggests that UGC 7321 may be a rather metal-poor galaxy (Goad & Roberts 1981), hence it might be argued that Galactic grain and extinction properties may not be applicable, and use of an alternate extinction curve [e.g., that from the Small Magellanic Cloud (SMC)] should be considered. However, we emphasize that adoption of an SMC-type extinction curve (e.g., Bouchet *et al.* 1985) would have no significant effect on the results we present here. The Galactic and SMC extinction curves are nearly identical in the optical, and begin to deviate significantly only in the ultraviolet, i.e. at wavelengths shortward of those considered in the present work (see, e.g., Witt & Gordon 2000).

2.4. *The Model Galaxy: Basic Structural Parameters*

To constrain the total amount of dust opacity in a galaxy like UGC 7321, we begin by attempting to construct models (composed of dust, gas, and stars) that can reproduce the observed morphology of UGC 7321 in various wavebands. Important constraints are also placed on our models by the observed radial and vertical color gradients in UGC 7321, as described in detail below.

We built our initial model galaxy based on the global disk parameters of UGC 7321 measured by MGvD99 and Matthews (2000): disk scale length h_r=2.1 kpc (as measured in R band), disk scale height h_z=140 pc (as measured in H band), and inclination $i = 88°$. For simplicity it was assumed that these parameters have no wavelength dependence. An axisymmetric, exponential distribution was adopted along the radial and vertical directions for both the dust+gas and the stars, as in Eq. 1 & 2. Using alternate analytic forms to describe the vertical light distribution [e.g., a sech(z) or sech^2(z) function] would have no appreciable effect on the conclusions that follow.

The scale height of the dust was assumed to be one half that of the stars ($h_{z,d} = \frac{1}{2}h_z$; e.g., Evans 1994; Xilouris *et al.* 1997,1999), and the dust scale length was taken to be $h_{r,d}$=1.5 kpc based on the observed dust clump distribution in the WFPC2 imaging observations shown in Figure 1. Although a number of workers have now argued for dust scale lengths equal to (e.g., Wainscoat, Freeman, & Hyland 1989) or exceeding those of the stellar light (e.g., Xilouris *et al.* 1999), such dust distributions are inconsistent with the observed distribution of dust in Figure 1 (see also MGvD99).

The resolution of our models is set by the size of our density grid (200^3 cells). Although the full measured radial extent of UGC 7321 in the R-band is ≈8.1 kpc, in order to obtain good spatial resolution we truncated our model calculations at $R_{max} = \pm 3h_r$ =6.3 kpc. This yielded a spatial resolution of ∼60 pc/pixel in our finite 200^3 cubic model grid and provides a good match to the projected pixel size of our H-band images (∼53 pc) and to the clump sizes of $\sim 30 - 100$ pc inferred from the WFPC2 data in Figure 1 (see also Gallagher *et al.* 2000).

Because UGC 7321 is essentially a pure disk galaxy (see MGvD99), no bulge component was included. Also, no spiral structure was added to our present models. Although we cannot know the true face-on appearance of UGC 7321, several arguments suggest that it is unlikely to exhibit well-defined spiral structure (see MGvD99). Moreover, to first order, the effects of spiral structure are averaged over in edge-on galaxies (see Xilouris *et al.* 1997),

and Misiriotis *et al.* (2000) have shown via detailed models that derived dust and extinction parameters do not change appreciably if spiral structure is included.

3. SCATTERED LIGHT IMAGES AND COLOR GRADIENTS

As described above, we tested models for UGC 7321 using both clumpy and smooth dust and stellar emissivity distributions in order to assess the amount and distribution of dust that can best reproduce observations of the galaxy. In this section we examine the scattered light images, luminosity profiles, and color gradients predicted by various models, and compare them to the real observations.

3.1. *Smooth Models: Inputs and Results*

We began our modelling of UGC 7321 by generating a grid of models over a wide range of optical depths, and having purely smooth stars and dust. Because the smooth models are simpler (i.e., require fewer input parameters) than the clumpy models, these allow us to zero in on a suitable range of optical depths for modelling a diffuse, LSB galaxy like UGC 7321. Here we further examine four of these models, having edge-on B-band optical depths of $\tau_{e,B}$=0.4, 2.0, 4.0 and 8.0 respectively. In Figure 4 (left), we show the R-band scattered light images corresponding to these models.

An examination of Figure 4 shows that we appear to have bracketed a suitable optical depth regime for modelling UGC 7321, but that our smooth models offer a relatively poor match to UGC 7321 morphologically. The models overall lack the patchy light appearance of the real galaxy, and in addition, the $\tau_{e,B} \geq$4.0 models exhibit clear dust lanes in the R-band not seen in the real data. Even the $\tau_{e,B}$=2.0 model shows a brightness asymmetry about the midplane not seen in R-band observations of UGC 7321. It is clear that in spite of the fact that an edge-on viewing angle averages over many of the irregularities in the dust and stellar distributions, a purely smooth model is insufficient to fully reproduce the observed properties of UGC 7321. Therefore in the next section consider models including a clumpy ISM phase, as well as a clumped stellar component.

3.2. *Clumpy Models: Inputs*

In this section we investigate the effects of introducing a clumpy, 2-phase ISM as well as a partially clumped stellar distribution on our Monte Carlo models.

From our smooth models we have narrowed in on a range of optical depths of interest for modelling UGC 7321 ($\tau_{e,B} = 0.4 - 8.0$). As a next step, we must determine suitable values to use for the filling factor ff and density contrast parameter C for both the stars and and the dust (see Sect. 2.2).

We note that for a clumpy medium, the optical depth, τ, is formally somewhat ill-defined (see Witt & Gordon 2000). However, because our clumpy models are formulated such that for a given value of 'τ' they have *on average* the same disk mass as a smooth model with the same τ value (see Sect. 2.2), one can still characterize the medium in terms of what is effectively a mean optical depth; we hereafter refer to this quantity as $\bar{\tau}$.

The clump filling factor for the ISM in real galaxies is very uncertain, and has been the focus of several other studies (e.g., Witt & Gordon 1996; Bianchi *et al.* 2000). As examples, typical values of around $ff = 0.15$ were adopted by Kuchinski *et al.* (1998) and Witt & Gordon (2000), while values of 0.10-0.25 were chosen by Mihos, Spaans, & McGaugh (1999). However, due to the expected greater sparsity of molecular clouds in UGC 7321 compared with a higher surface brightness or Milky Way-like spiral, we feel the use of a somewhat lower filling factor of denser clumps is warranted. After trial and error, for the present case we find a value of $ff_{gd} = 0.06$ to be suitable.

The parameter C for the ISM is also somewhat uncertain. We therefore tested models with C=100,40,20,9, & 2 in order span the range of values suggested by other workers for different environments, from Milky Way-like galaxies (e.g., Witt & Gordon 1996; Mihos, Spaans, & McGaugh 1999) to LSB galaxies (e.g., Mihos, Spaans, & McGaugh 1999). Our choices of C correspond to ratios of clumpy to smooth mass of 86:14, 72:28, 56:44, 36:64, & 25:75, respectively. In the present case, we found the best qualitative matches to the data with C=20. Models with less than ∼50% of the opacity in a clumped medium produced image morphologies too smooth to match the data, while clumpier models tend to produce an overly mottled morphology.

Having established estimates of the ISM parameters, we first ran a grid of models for various optical depths containing a clumpy ISM but purely smooth starlight. Once again, the resulting model images appeared too smooth to match the real data. Therefore these models are not discussed further here. Not surprisingly, we find that a partially clumped stellar distribution in combination with a multi-phase ISM will be required to realistically model UGC 7321.

To model a clumped emissivity distribution, we must now also choose appropriate values of C_* and ff_* for the stellar component of our models. In this case, we chose several values of C_* in the range representing rough approximations to the total amount of starlight from star-forming regions versus smooth underlying disk regions that one might expect to see in real LSB galaxies. We then ran grids of models with different stellar filling factors ff_* until we found good matches to the observed image morphologies of UGC 7321 in the B, R, and H bands. We viewed each of our models from both an $i = 88°$ and a face-on orientation to check that our model looked qualitatively like a real late-type LSB galaxy disk from multiple viewing angles. Through this scheme we arrived at preferred values of ff_*=0.60 and C_*=2. This results in an apportionment of ∼75% of the light into higher density component and ∼25% into a smooth background component. However, we emphasize that none of our key conclusions regarding the total amount of dust in UGC 7321 or its corresponding effects on the observed properties of the galaxy are strongly sensitive to the choice of these values.

Lastly, we note that one might expect some small wavelength dependence on C_* and ff_* to account for the fact that generally the starlight in galaxies becomes intrinsically smoother as one moves from the optical to the NIR regime. However, as shown by Bergvall *et al.* (1999), LSB galaxies tend to exhibit relatively minor morphological differences between the optical and NIR compared with brighter spirals. Therefore we have settled on one value of

ff_* and of C_* that appear to give satisfactory matches to the data over the range of wavelengths considered here.

3.2.1. *Scattered Light Images from the Clumpy Models*

R-band scattered light images for our grid of clumpy models with $\bar{\tau}_{e,B}$=0.4, 2.0, 4.0, and 8.0 are shown in Figure 4 (right), alongside the smooth models from Sect. 3.1 for comparison. It is immediately clear that unlike the smooth models, our clumpy models do not exhibit dust lanes within this range of optical depths. Rather one sees the signatures of clumpy, irregular absorption over the central few kpc of the galaxy, consistent with the real UGC 7321. All models also show a much less pronounced asymmetry about the midplane compared with the smooth models of the corresponding optical depth. In addition to the models shown in Figure 4, we also ran clumpy models with $\bar{\tau}_{e,B}$=12 and 24, but these models showed clear dust lanes and could be immediately ruled out as having too much opacity.

Of the models shown in Figure 4, the $\bar{\tau}_{e,B}$=4.0 case appears to provide the best fit to multiwavelength observations of UGC 7321 on a purely morphological basis. In the $\bar{\tau}_{e,B}$=8.0 model, we see too few bright emitting regions more than one pixel across, and somewhat too much central opacity. In contrast, the $\bar{\tau}_{e,B} = 0.2$ and 2.0 models both show stronger central concentrations of starlight at R-band than in the real galaxy, and less patchiness within the inner few kpc. The $\bar{\tau}_{e,B}$=4.0 has a discernible but weak central concentration of starlight, and little evidence for absorption outside roughly $\pm$3 kpc, both in excellent agreement with UGC 7321. The match of the $\bar{\tau}_{e,B}$=4.0 model is also quite good at H-band, where it nicely reproduces the more well-defined brightness center of the galaxy and overall smoother appearance of the central regions of the galaxy as seen at these wavelengths. In Figure 5 we show more detailed close-ups of the $\bar{\tau}_{e,B}$=4.0 R and H scattered light images compared with view of the real galaxy at the corresponding wavelengths.

3.3. *Color Gradients Predicted from Clumpy Models*

We now explore the color gradients predicted by our models and compare them to those seen in the real data. In Figure 6 we plot the $B-R$ and $R-H$ radial color gradients along the major axis extracted from both our smooth models (from Sect. 3.1) and our clumpy models, for the optical depths $\tau_{e,B}$=0.4, 2.0, 4.0, and 8.0. As expected, the color profiles extracted from the clumpy models appear somewhat "noisier" than those from the smooth models. In fact, the intrinsic rms noise inherent in our models in only $\sim$0.005 magnitudes, hence the visible fluctuations in the radial color profiles in the lower portion of Figure 6 are real.

From Figure 6 we see that at a given optical depth, the total dust-induced color gradient (from disk edge to center) is virtually identical to that in the smooth models. Likewise, the *mean* amount of reddening at a given galactocentric radius is nearly identical in the two sets of models; along a given sight line, differences appear to be $\leq$0.015 magnitude. In general, the reddening effect of a clumpy medium is expected to be smaller than that produced by a diffuse model with the same amount of dust, particularly if the filling factor of the clouds is small (e.g., de Jong 1996; Bianchi *et al.* 2000). However, our new models show that in the low optical depth regime, even for the low clump filling factors used here, this effect is nearly imperceptibly small, and that both the clumpy and the smooth models produce roughly the same amount of *mean* reddening, albeit with much larger statistical variations between different lines of sight. We find this holds even for a pure clumped medium with no smooth component.

A further examination of Figure 6 reveals that the observed $\Delta(R-H)$ $\sim$0.9 of Figure 3 cannot be reproduced solely from dust effects for models with $\tau_{e,B} \leq 8.0$. Meanwhile, the $B-R$ color profiles for both the smooth and the clumpy models over this optical depth range show an additional interesting behavior: for $\tau_{e,B}$ $\geq$4.0 the dust-induced $B-R$ color actually *saturates* at $\Delta(B-R)$ $\sim$0.31. In other words, adding additional dust cannot further increase the total dust-induced $B-R$ color gradient to $>$0.31 magnitudes from the disk edge to the disk center. As seen from Figure 2, $\Delta(B-R)$ $\sim$0.3 is significantly less than the actual observed $B-R$ color gradient in UGC 7321 over this radial interval, hence our models indicate that no amount of dust can fully account for the observed $B-R$ color gradient in UGC 7321.

This saturation effect we see in the dust-induced $B-R$ color gradients arises due to the wavelength-dependent absorption in realistic systems where emission and absorption are mixed together (in contrast, for example, to simple foreground screen models). A simple illustrative example is a constant density absorbing medium (no scattering) with uniform emissivity, i.e., a slab model where the stars and dust are spatially coincident. The emergent intensity is $I_\lambda \propto [1-e^{-\tau_\lambda}]/\tau_\lambda$. From Table 2, we see that (approximately) $\tau_B : \tau_R : \tau_H = 8:4:1$, giving

$$\frac{I_B}{I_R} \propto \frac{[1-e^{-\tau_B}]}{2[1-e^{-\tau_B/2}]}\ , \quad \frac{I_R}{I_H} \propto \frac{[1-e^{-\tau_B/2}]}{4[1-e^{-\tau_B/8}]}\ . \qquad (5)$$

Plotting $(B-R)$ and $(R-H)$ against τ_B for this simple example (Figure 7), we see that $(B-R)$ saturates before $(R-H)$ due to the smaller opacity difference in going from B to R, than in going from R to H. The exact optical depth at which the saturation occurs is slightly different for this simple model than the more realistic models we have computed. However it still demonstrates that even if we have significantly underestimated the amount of opacity in UGC 7321's disk, our conclusion remains unchanged that dust alone still cannot account for the large color gradients observed in UGC 7321.

Above we have argued that models for UGC 7321 with $\bar{\tau}_{e,B}$ $\geq$8.0 can be ruled out on a purely morphological basis. To further demonstrate that we have not grossly underestimated the amount of internal extinction in UGC 7321, we have also examined the $H-K$ color gradients. In Figure 8 we show the $H-K$ color profile along the major axis for our family of clumpy models, and in Figure 9 we show a radial $H-K_s$ color plot for UGC 7321 derived from 2MASS data. The field-of-view of the available 2MASS data is limited to $\sim 200''$, and due to the large angular size of UGC 7321 compared with the scan size of the survey, the data have very poor signal-to-noise outside the central arcminute or so of the galaxy (see Jarrett *et al.* 2000 for an description of 2MASS extended source data). Nonetheless, the 2MASS data are consistent with a $H-K$

radial color gradient of no more than ∼0.1 magnitude in UGC 7321. Comparing this to our models, we see that $\bar{\tau}_{e,B}$=8.0 models produce a $\Delta(H-K)$ in excess of that expected on the basis of the 2MASS results.

As a final test on our estimates of τ, we lastly examine the *vertical* $B-R$ color gradients (i.e., those parallel to the minor axis) for the same four optical depths as above (Figure 10) and compare these with the real data (Figure 11).

In the real UGC 7321 data, near the minor axis, the vertical $B-R$ color profile is seen to be redder by ∼0.31 magnitudes at z=0.15 kpc compared to the highest observable z-heights (Figure 11). However, we see that the $\bar{\tau}_{e,B}$=8.0 model predicts a reddening of several tenths of a magnitude higher than this along the minor axis. Meanwhile, since reddening toward the midplane along the z direction is in general due to dust rather than stellar population effects, it appears $\bar{\tau}_{e,B}$ >2.0 is required in order to explain the amount of reddening that is observed. Hence we again conclude that the $\bar{\tau}_{e,B}$=4.0 model produces the best overall match to the data.

Near a galactocentric radius of 1.′0 (∼3 kpc), the $\bar{\tau}_{e,B}$ = 4.0 model predicts a dust-induced vertical $B-R$ color gradient of ∼0.15 magnitudes. In the real UGC 7321 data, MGvD99 actually observed a *bluing* of $\Delta(B-R)$ ∼0.3 toward the galaxy midplane at this radius. Such a bluing toward low z-heights is predicted to occur as a consequence of new young stars continually being born near the galaxy midplane, while older stars are scattered to larger z heights via dynamical heating processes (e.g., Just, Fuchs, & Wielen 1996). The small amount of dust reddening helps to explain why UGC 7321 is one of the few galaxies studied so far in which we can readily observe the predicted stellar population changes with z-height. This demonstrates that edge-on LSB galaxies like UGC 7321 can provide excellent laboratories for further constraining dynamical heating processes.

In summary, we conclude that *a clumpy ISM model with* $\bar{\tau}_{e,B}$ *∼4.0 provides the best characterization of the observed properties of UGC 7321, and that dust alone cannot account for the large radial color gradients observed in this galaxy.* This suggests that the existence of significant stellar population gradients (and possibly metallicity gradients) in the disk of UGC 7321, and the likelihood that galaxies like UGC 7321 maintain a well-preserved record of how galaxy disks have been built up over time.

3.4. *Radial Intensity Profiles*

In Figure 12 we show B, R, and H radial brightness profiles extracted along the major axes for our grid of clumpy models. These profiles permit estimates of the expected extinction along different lines of sight and in different wavebands for a galaxy like UGC 7321. These profiles confirm that for a $\bar{\tau}_{e,B}$=4.0 model, extinction effects are nearly negligible in H-band, even at small galactocentric radii (see also MGvD99; Matthews 2000). They also show that in B-band, extinction toward the the center of UGC 7321 should be roughly 0.65±0.2 magnitudes in B-band and 0.43±0.2 magnitudes in R, in good agreement with the estimates made by MGvD99.

3.5. *UGC 7321 Analogs at Other Inclinations*

We have seen from our models in the previous sections that UGC 7321 is dust poor, but not dust free, and that small but non-negligible corrections must be made for the total internal extinction and reddening caused by dust when interpreting the colors, total magnitudes, and intrinsic surface brightnesses of LSB galaxies viewed at high inclination. But what about at lower inclinations?

An advantage of our 3D Monte Carlo simulations is the ability to easily examine a given model at any arbitrary viewing angle. We can therefore use the models described above to predict how dust will affect the observed properties of LSB disk galaxies seen at inclinations higher or lower than 88°. Other authors have previously used Monte Carlo simulations to explore the effects of dust on the colors and global extinctions of less inclined galaxies (e.g., de Jong 1996), but our high resolution, high signal-to-noise simulations allow us to probe the detailed effects of dust on the observed light and color distributions in the very low optical depth regime appropriate for LSB galaxies and also to investigate the effects of a clumpy ISM. All of the models we discuss in this section have stellar and dust scale parameters identical to those used in the UGC 7321 models of the previous sections (see also Table 2).

In Figure 13 & 14 we show the predicted $R-H$ and $B-R$ major axis color profiles for our $\tau_{e,B}$=0.4-8.0 smooth and clumpy models, respectively, at inclinations i = 0°, 45°, and 90°. For comparison, we also replot our i = 88° models from Figure 6.

At i = 90°, the observed trends are much as expected. For the various optical depths, we see small increases of order 0.1 magnitude in the amplitude of the $R-H$ color gradients compared with the i = 88° models, and difference of ∼ 0.05 magnitude in $\Delta(B-R)$ compared with the i = 88° case. The effects at i = 0 and i = 45° are somewhat more interesting, although primarily from a theoretical perspective. In cases of galaxies viewed at high inclinations, light scattered by dust has only a small effect on the emergent light profiles, particularly in a clumpy medium. Instead the observed color changes are dominated by dust absorption effects. In contrast, for $i \leq 45°$ and the small optical depths we consider here, we can see directly from our models how the dominance of scattering versus absorption changes across the face of the galaxy. In these cases, dust scattering actually causes a *bluing* of the light towards the galaxy center. For the higher optical depth ($\tau_{e,B}$ ≥2.0) models, this trend is interrupted by a rather abrupt reddening at the smallest galactocentric radii. These trends are easier to see in the smooth models (Figure 13). However, note that at both i = 0 and i = 45°, the maximum amplitude of these effects are only a few hundredths of a magnitude and therefore are predicted to essentially unobservable in real LSB galaxies. We conclude that at low and moderate optical depths, dust will have no appreciable effect on the observed radial color gradients of moderately inclined galaxy disks, consistent with the findings of de Jong (1996). Likewise, internal extinction corrections at optical and NIR wavelengths should be almost negligible for the bulk of LSB galaxies viewed at low or moderate inclinations.

3.6. *Discussion*

3.6.1. *Gas-to-Dust Ratios and Total Dust Content*

In Sections 3.2.1 & 3.3, we concluded that among the models we have considered, a clumpy, multi-phase ISM model with $\bar{\tau}_{e,B} \approx 4.0$ provides the best overall match to the observed properties of the edge-on LSB galaxy UGC 7321. We now consider some additional implications of this model.

As described in Sect. 2.2, we have parameterized our models in terms of the opacity of a gas+dust mixture. For a given optical depth, the total mass of material in our model ISM can then be computed as

$$M_{ISM} = \int \rho \mathrm{dV} = \tag{6}$$

$$2\pi\rho_0 \int_{-\infty}^{\infty}\int_{0}^{R_{max}} \exp\left(\frac{-r}{h_{r,d}} - \frac{|z|}{h_{z,d}}\right) \mathrm{d}z r \mathrm{d}r \approx 4\pi\rho_0 h_{r,d}^2 h_{z,d}$$

From this, one can obtain the mass in the form of dust by dividing Eq. 6 by the assumed gas-to-dust ratio of the absorbing medium (in our case, ρ_g/ρ_d=140; see Sect. 2.3). In terms of the edge-on optical depth $\tau_{e,B}$, the dust mass M_d can thus be expressed in solar units as

$$M_d = 2.2 \times 10^7 \cdot (\rho_g/\rho_d)^{-1}\, \tau_{e,B} \quad M_\odot. \tag{7}$$

For our $\bar{\tau}_{e,B}$=4.0 clumpy models, this yields $M_d \sim 8.8 \times 10^5$ $\mathcal{M}_\odot$, with 56% of this in a clumpy component, and the remainder in a smoothly distributed medium.

IRAS far-infrared flux measurements are also available for UGC 7321 (e.g., Sage 1993), allowing an independent estimate of the dust content of UGC 7321. From the *IRAS* 100μm flux, one can make an estimate of the mass of the far-infrared-emitting dust in a galaxy as:

$$M_{d,100\mu\mathrm{m}} = c_g S_{100} D^2 (e^{144/T_d} - 1) \quad M_\odot \tag{8}$$

where S_{100} is the *IRAS* 100μm flux density in Jy (1.15 Jy for UGC 7321; Sage 1993), D is the distance in Mpc, T_d is the dust temperature, and c_g is a constant that depends on the grain opacity, and can vary by roughly a factor of two, depending on the composition of the grains (e.g., Devereux & Young 1990). Sage (1993) estimated T_d=33.5 K for UGC 7321, and we adopt the value of c_g=5 suggested by Thronson & Telesco (1986). This yields $M_{d,100\mu\mathrm{m}} \sim 4.2 \times 10^4$ $\mathcal{M}_\odot$ for UGC 7321, or only ∼5% of the dust mass estimated from our models. However, Devereux & Young (1990) found from an examination of a large sample of *IRAS*-detected nearby galaxies, that typically only ∼10-20% of the total dust mass in normal disk galaxies is warm enough to radiate in the *IRAS* bands (see also Greenberg & Li 1991; Whittet 1992). Lisenfeld & Ferrara (1998) also found for a sample of dwarf galaxies that the dust mass derived from extinction estimates is on average ∼ 29× lower than that derived from FIR data. If this also holds for UGC 7321, then our estimated dust mass from our models appears to correlate roughly as expected with the estimate from the *IRAS* data, especially given the uncertainties in the *IRAS* estimate (see, e.g., Lisenfeld & Ferrara 1998).

Let us now return to the issue of the total interstellar gas mass implied by our models. As described in Sect. 2.2, our models are parameterized in terms of a total opacity and assume gas-to-dust ratio of 140 (Kim, Martin, & Hendry 1994). As emphasized earlier, although the exact choice of the gas-to-dust ratio has negligible effect on the extinction and reddening parameters derived from our models (since the opacity of the gas is negligible), it does however impact the total gas+dust mass we infer: for ρ_g/ρ_d=140, we derive from Eq. 6 $M_{ISM} \approx 1.2 \times 10^8$ for our $\bar{\tau}_{e,B}$=4.0 model.

H I spectral line measurements by MGvD99 yield a total integrated H I mass for UGC 7321 of $\mathcal{M}_{HI}$=1.1×10^9 $\mathcal{M}_\odot$. Devereux & Young (1990) found that typically only the H I gas contained within roughly half of the optical radius of spiral galaxies has appreciable dust associated with it. From the pencil beam map of MGvD99, we estimate this corresponds to ∼50% of the total H I content of UGC 7321, or ∼5.5×10^8 $\mathcal{M}_\odot$. In addition, Matthews & Gao (2000) recently detected ^{12}CO 1→0 emission from the central regions of UGC 7321, and estimated a molecular hydrogen content within the central 2.5 kpc of the galaxy of $\sim 2 \times 10^7$ $\mathcal{M}_\odot$ using a standard Galactic CO-to-H_2 conversion factor (but see below). Thus after correction for helium, the total gas content in the central regions of UGC 7321 is ∼6.2 times *more* than the total ISM mass inferred from our models. This discrepency is significant even after accounting for the range of accepted values for the Galactic gas-to-dust ratio [where ρ_{gas}/ρ_{dust} ∼120-140 based on depletion and extinction measurements (Whittet 1992)]. Not surprisingly, *the assumption of a Galactic gas-to-dust ratio appears to be invalid for UGC 7321.*

There is now considerable evidence that the gas-to-dust ratio varies from galaxy to galaxy (e.g., Bouchet *et al.* 1985; Hunter *et al.* 1989; Dwek 1998; Lisenfeld & Ferrara 1998), with position within galaxies (e.g., Stanimirovic *et al.* 2000), and as a function of metallicity (e.g., Bouchet *et al.* 1985; Lisenfel & Ferrara 1998). For example, Koornneef (1982) found the gas-to-dust ratio for the Large Magellanic Cloud (LMC) to be ∼4 times the Galactic value, while Bouchet *et al.* (1985) and Stanimirovic *et al.* (2000) found a value for the SMC of ∼8-11 times Galactic (assuming a Galactic gas-to-dust ratio of ∼140).

Although no oxygen abundance measurements are available for UGC 7321, typical metallicity values for LSB galaxies tend to be $\lesssim$ 1/3 solar (e.g., McGaugh 1994; Rönnback & Bergvall 1995). That we require a gas-to-dust ratio of ∼6.2 times the Galactic value to reconcile our model gas masses with observed values of UGC 7321 thus seems appropriate for a galaxy whose metallicity is likely to lie somewhere between SMC and LMC values. The *global* gas-to-dust ratio inferred from our extinction estimates and the total observed H I content of UGC 7321 (after correction for He) would then be ∼1600.

3.6.2. *Implications of a Clumpy, Multi-Phase ISM in UGC 7321*

We have shown that a dusty ISM with a significant fraction of its total mass (∼56%) in a the form clumpy component is needed to explain the observed properties of UGC 7321. We now consider the implications of such a finding.

For the type of simple, two-phase ISM model that we have used in the present work, it is often assumed that the clumped component of the medium should represent a predominantly molecular gas medium, while the diffuse component represents diffuse atomic gas (e.g., Bianchi *et al.*

2000). In the case of UGC 7321, if we make such assumptions, then we would predict a molecular gas to atomic gas ratio somewhat higher than the typical upper limits of $\lesssim$40% found for the central regions of Sd-Sdm galaxies by Devereux & Young (1990). Moreover, this is considerably higher than empirical measures for UGC 7321 by Matthews & Gao (2000), which suggest that only $\sim$4% of the total gas content in the central regions of UGC 7321 is molecular (assuming a Galactic CO-to-H_2 conversion factor).

There are several possible explanations for this trend. Firstly, the association of the atomic gas solely to a diffuse component, and the molecular gas solely to the clumped component in a gross oversimplification of the ISM of any galaxy (e.g., Turner 1988; Elmegreen 1993). This may be particularly true in the interstellar environments of LSB galaxies. The optical depths we infer for the "dark clouds" in UGC 7321 ($A_V \lesssim 1.5$; see also Gallagher *et al.* 2000) are consistent with the diffuse molecular clouds, and the lowest density Giant Molecular Clouds in the Milky Way (cf. Turner 1997). It has been suggested that such dark clouds in galaxies like the SMC may in fact contain significant atomic components (e.g., Dickey 1996; Kenney 1997). Even if such clouds are primarily molecular, their lower densities imply long timescales for the formation of CO molecules, and hence a reduction in the size of the CO-emitting regions within clouds of a given radius (e.g., Maloney 1990). In this case, CO measurements will significantly underestimate the molecular gas content of the clouds. Further uncertainties in the empirical H_2 estimate come from possible metallicity dependence on the CO-to-H_2 conversion factor (e.g., Maloney 1990). A final possibility is that the gas-to-dust ratio differs between diffuse and clumpy ISM regions regions. This could occur, for example, if dust is accreted onto denser clouds, while dust in the diffuse medium is destroyed by shocks on timescales much shorter than new dust grains are created (e.g., Tielens 1998), although others have argued that gas and dust should be generally well mixed in the ISM (e.g., Cox & Mezger 1989).

Regardless of the exact atomic versus molecular fraction in the clumpy ISM of UGC 7321, its very existence has interesting implications for furthering our understanding of the conditions in the ISM of LSB galaxies. Previously, it has been suggested that it is likely that interstellar pressures in LSB galaxies would be too low to sustain a multi-phase structure in the diffuse, low metallicity environments in LSB galaxies (Mihos, Spaans, & McGaugh 1999). Our data and models confirm that at least some LSB galaxies can maintain sufficient pressures to support a modest, multi-phase ISM. In addition, the existence of dust in ISM regions of enhanced density suggests that LSB galaxies have the envionments and the catalysts needed for molecular hydrogen formation.

In general, a clumpy ISM should support higher H_2 fractions than a nearly smooth ISM due to the presence of more efficient shielding of molecules from ionizing radiation fields (see also Spaans 1998). Thus even if the dark clouds in UGC 7321 contain significant atomic components, their inner regions almost certainly contain molecular cores (as confirmed by the CO detection of Matthews & Gao), hence eliminating the need to invoke star formation in LSB galaxies directly from atomic gas (cf. Schombert *et al.* 1990). This also raises the probability that other LSB galaxies could be detected in CO with sufficiently deep integrations (see also Matthews & Gao 2000).

4. MODEL ROTATION CURVES

4.1. *Background*

4.1.1. *The Importance of LSB Galaxy Rotation Curves*

Because of their relatively low visible matter contents relative to their inferred dynamical masses, LSB galaxies offer an important class of objects for unravelling the nature of dark matter in galaxies, as well as for testing dark matter alternatives, such as Modified Newtonian Dynamics (MOND; Milgrom 1983). An important step in this process is deriving accurate rotation curves.

For some applications, systems that are nearly edge-on can be particularly desirable for rotation curve studies since inclination corrections to line-of-sight velocities and position angle uncertainties in these cases are small. H II regions can also in general be observed to larger galactocentric radii in edge-on galaxies than in less highly inclined systems, and edge-on galaxies are much easier to pick out and observe at higher redshifts.

Unfortunately, the interpretation of observed rotation curves via mass-modelling techniques (e.g., Carignan 1985) is strongly dependent on knowledge of the precise shape of the inner, rising portion of the rotation curve. This is often poorly determined observationally, particularly in edge-on galaxies. If rotation curves are derived from H I data, they often suffer from beam smearing (see, e.g., Swaters 1999 and references therein; van den Bosch *et al.* 2000). High spatial resolution optical data can overcome this problem, but instead suffer from the vagaries and uncertainties of internal absorption in a given galaxy, and the debate over how accurately H II regions trace the true disk rotation (e.g., Davies 1991; Prada *et al.* 1994; McKeith *et al.* 1995; Prada 1996). Uncertainties due to projection effects and unknown gas distributions will also plague the interpretation of both optical and H I data in the edge-on case.

Our Monte Carlo simulations provide a means to derive model optical rotation curves for edge-on galaxies and to test the severity of some of the influences mentioned above. Bosma *et al.* (1992) and Bosma (1995) have already shown via rotation curve models and a comparison between H I-, CO-, and optically-derived rotation curves that even edge-on galaxies tend to be largely optically thin. Bosma *et al.* (1992), Byun (1993), and Bosma (1995) also showed that extremely high optical depths are needed to produce an apparent linear rotation curve from an intrinsically steeply rising one, even in edge-on and nearly edge-on galaxies. Here we reconfirm their results via Monte Carlo techniques, and also concentrate more specifically on exploring situations relevant to the interpretation of the rotation curve data for edge-on and nearly edge-on LSB galaxies, including UGC 7321. We also assess the promise of using such systems for detailed dynamical studies and mass modelling.

4.2. *Artificial Rotation Curves: the Method*

For the present study, we model galactic rotation curves by inputting an analytic galactic rotational law for our

model galaxy, and then adding together the Doppler shifts that arise between the emitted photons (presumed to arise from Hα-emitting "H II regions") and the observer. We found that also including the Doppler shifts arising from the relative bulk motions of the scattering dust particles had negligible effect on the final rotation curves (see also Bosma *et al.* 1992). We assume that the dust opacity is constant over the narrow wavelength range that an observer would use to trace the galactic rotation. Because we are keeping track of wavelength in these simulations, when a photon exits the galaxy we project the photon into an image, and form "channel maps" by assigning an image to a particular wavelength range.

The output of our radiation transfer code is a 3D data cube consisting of N two-dimensional channel maps. To form a rotation curve from our channel maps we take a strip across the major axis of each channel map and calculate the flux-weighted velocity at each position along the strip

$$v(x) = \sum_{i=1}^{N} v_i F_i(x) / \sum_{i=1}^{N} F_i(x) \ , \qquad (9)$$

where x is the position along the "slit", v_i is the velocity corresponding to the ith image channel, and $F_i(x)$ is the flux at position x in the ith image channel. We note that this type of intensity-weighted determination of $v(x)$ is technically correct only for non-edge-on galaxies (e.g., Sancisi & Allen 1979). However, it is still most commonly the method employed by optical observers of edge-on galaxies (e.g., Goad & Roberts 1981; Karachentsev & Xu 1991; Makarov, Burenkov, & Tyurina 1999; Dalcanton & Bernstein 2000), hence we adopt it here for ease of comparison of our models with data from the literature. The intrinsic spectral resolution of our models is 4.5 km s^{-1} pixel^{-1}. Before plotting our model rotation curves, we convolved them with Gaussians representing the expected turbulence of the ionized gas (assumed to have σ=10 km s^{-1}) and a typical instrumental resolution (taken to be 30 km s^{-1}). For simplicity, we begin by exploring smooth emissivity distributions. The case of clumpy emissivity is explored in Sect. 4.3.3.

4.3. *Artificial Rotation Curves: the Models*

As discussed above, the shape of the rotation curve observed for an edge-on galaxy at optical wavelengths may arise from a combination of effects, including: (1) the intrinsic shape of the underlying rotation curve; (2) projection effects; (3) dust extinction; (4) anomalously high extinction in the center only; (5) a complete absence of ionized gas in the central regions; (6) clumpy or irregularly distributed gas. Here explore the consequences of these effects for the observed rotation curves of edge-on galaxies similar to UGC 7321.

4.3.1. *Effects of Internal Extinction, Projection, and Intrinsic Rotation Curve Shape*

Let us first consider models that explore items (1)-(3) listed above, i.e., intrinsic rotation curve shape, projection effects, and wide-spread dust extinction.

We take UGC 7321 as our template galaxy, adopting in all of our model rotation curves its inferred dust model distribution from Sect. 2.4 & 3.2, and a maximum rotational velocity of 100 km s^{-1} (MGvD99). For simplicity, we assume the scale height and scale length of the Hα corresponds to that of the stars.

We begin with the simple case of a smooth dust emissivity distribution and consider edge-on optical depths of $\tau_{B,e}$=0,2.0, and 100. We compute our models for three inclinations: $i = 85°$,88°, and 90°. As already shown by Bosma *et al.* (1992), the effects of items (1)-(3) above begin to become negligible at inclinations $i \lesssim 85°$.

For our input rotation laws, we choose four different rotation curve shapes. Three of the forms are based on the observed rotation curves of edge-on galaxies in the literature having luminosities and peak rotational velocities similar to UGC 7321. The adopted models are (*i*) a very steeply rising curve, rising linearly to V_{max} within 0.25 kpc and staying flat thereafter; (*ii*) a moderately steep curve, rising linearly to V_{max} within the inner 1 kpc and flattening thereafter (e.g., UGC 3697, Goad & Roberts 1981); (*iii*) an "arctan" rotation curve (see Courteau 1998) of the form $v(R) = v_0 + \frac{2}{\pi} v_c \arctan(R)$ where $R = (r - r_0)/r_t$, v_0 is the velocity center of rotation, r_0 is the spatial center of the galaxy, v_c is an asymptotic velocity, and r_t is a transition radius between the rising and flat parts of the rotation curve (e.g., UGC 7321; Goad & Roberts 1981). For the arctan model we adopt v_0=0, v_c=100 km s^{-1}, r_0=0, and r_t=1.3 kpc. Finally (*iv*) is a rotation curve that rises linearly to $2.2h_r$ and has only an essentially negligible flat portion within the stellar disk (see UGC 9242, Goad & Roberts 1981; FGC 1285, Dalcanton & Bernstein 2000).

Our resulting models for these four different rotation curve shapes at three inclinations and three different optical depths are illustrated in Figure 15. In Figure 16 we also show $\tau_{e,B}$=4.0 models for input rotation curve forms (*ii*) and (*iii*) with the Hα emission line data from Goad & Roberts (1981) overplotted.

Several interesting trends are immediately evident in Figure 15. First, our model curves reconfirm the result of Bosma *et al.* (1992) that an observed rotation curve that is linear and rising to the outer regions of the stellar disk cannot be produced by any physically plausible amount of internal extinction. For $i = 88°$, we find that edge-on optical depths of $\tau_{B,e} \gtrsim$100 are needed to produce such an observed rotation curve for any type of intrinsic rotation curve shape resembling models (*i*)-(*iii*)–i.e. for any shape other than an intrinsically slowly rising one. Moreover, it becomes clear from Figure 15 that such a linear shape cannot be solely the result of deriving the rotational velocities via "intensity-weighted" procedures. We conclude that edge-on galaxies exhibiting linear, slowly rising rotation curves throughout their stellar disks (e.g., UGC 9242, Goad & Roberts 1981; FGC 1285, Dalcanton & Bernstein 2000) must necessarily be galaxies with low central matter densities and are likely to generally be optically thin systems. In the low optical depth regime appropriate for a typical LSB galaxy ($\bar{\tau}_{B,e} \sim$4; see Sect. **??**), the effects of dust extinction on the observed rotation curve are small enough to be safely ignored even in the case of $i = 90°$.

At the opposite extreme, if a very steeply rising rotation curve that flattens appreciably in the inner few kpc is directly observed in a highly inclined galaxy (e.g., UGC 3697; Goad & Roberts 1981), Figure 15 shows that one can infer that not only must the galaxy be relatively optically thin, but it must also be inclined at an angle

$i \lesssim 85°$ in order for its steep rise to be preserved in projection.

Figure 16 illustrates that either of the two intermediate models [(*ii*) or (*iii*)] provides a roughly equally good match to the overall shape of the UGC 7321 rotation curve as measured by Goad & Roberts (1981), allowing for observational uncertainties and a slight lopsidedness in the true rotation curve. Thus we see that in these intermediate regimes, recovering the true, underlying rotation curve shape for a particular galaxy is less clear-cut. All of our models show that for the optical depths appropriate for a galaxy like UGC 7321, the effects of extinction can be safely ignored; instead, the greater ambiguity arises from the fact that rotation curves of quite different shapes, steepnesses and turnover radii can look very similar in projection if the galaxy inclination angle $i > 85°$. Hence, this could create a much more serious problem for an observer attempting a dynamical model of a galaxy like UGC 7321. In the case where the inclination is not precisely known, the ambiguity becomes even more severe.

4.3.2. *Effects of Galaxy Centers Devoid of Gas*

It is sometimes suggested that the linear or slowly rising rotation curves of some edge-on galaxies are due not to high optical depths throughout the disk, but rather a dearth of gaseous material in the inner regions of the galaxy, or the possibility that the H II regions (or H I gas) are confined primarily to a ring-like distribution. The former case is essentially equivalent to a galaxy which for some reason may have a high optical depth near its center, but still may have an optically thin outer disk (cf. Davies 1991). Using our models, we explore the applicability of such models to UGC 7321, and to explaining the linear, slowly rising rotation curves seen numerous late-type, edge-on galaxies (e.g., Goad & Roberts 1981; Karachentsev & Xu 1991; Makarov *et al.* 1997; Makarov, Burenkov, & Tyurina 1999; Dalcanton & Bernstein 2000).

We are immediately able to rule out a pure H II region "ring" model for UGC 7321, and indeed, for most late-type, edge-on galaxies where Hα imaging data are available. Such a ring morphology creates an Hα intensity distribution with peaks at the galactocentric radii corresponding to the radius of the projected ring; such a distribution is inconsistent with Hα imaging data available for UGC 7321 (MGvD99), for several other superthin galaxies (Rönnback & Bergvall 1995; Hoopes, Walterbos, & Rand 1999; Matthews *et al.* unpublished) and for numerous less inclined LSB disk galaxies (e.g., Schombert *et al.* 1992; O'Neil *et al.* 1998).

Although the ring model seems implausible, MGvD99 did report a paucity of Hα emission near the center of the UGC 7321 disk, suggesting the possibility of a gas-poor or high optical depth region in the inner 0.5 kpc or so of the galaxy. For illustration purposes, here we test a somewhat more extreme version of this model. In Figure 17, we show a model for $i = 88°$ and rotation curve model (*ii*), but this time the model galaxy is completely devoid of Hα emission within a central hole of radius 1.5 kpc. All other parameters are as in the models in Figure 15.

It can be seen in Figure 17 that the effect of this Hα-poor central disk region is to make the slope of the rotation curve slightly shallower than the case where the emission extends all the way to the center (cf. Figure 15). However, this is still not sufficient to produce a linear rotation curve shape. The effect would of course increase somewhat if the hole were made larger, but such a model seems highly contrived; we are aware of no examples of Sd spiral galaxies devoid of Hα emission over such a large fraction of the disk, nor should optical depth effects completely prevent Hα from being observable at small radii in normal late-type spirals, particularly LSBs. Hence this model should illustrate the upper limit of this effect for a realistic Sd galaxy. We conclude that the uncertainty of how far the emitting gas extends to the center of a galaxy will create additional small uncertainties in uncovering the the intrinsic inner rotation curve shape for galaxies with $i \geq 85°$. However this effect cannot in itself produce an apparent linearly rising rotation curve for physically realistic galaxy models.

4.3.3. *The Effects of Clumpy of Sparsely Distributed H II Regions*

Up until now, we have considered only smooth emissivity distributions for our rotation curve models. However, the H II regions from which a rotation curve would be derived in a real galaxy are likely to have a clumpy and somewhat irregular distribution. Their distribution may be particularly sparse or irregular in the case of LSB galaxies (cf. Schombert *et al.* 1992; O'Neil *et al.* 1998). To explore how this may affect an observed rotation curve, we now compute a model where the Hα filling factor $ff_{H\alpha}$ is only 0.5% and where $C_{H\alpha}$=100.

In Figure 18 we show these "clumpy" models for the $i = 88°$ case and input rotation curve form (*ii*). As expected, the models now show a much more ragged appearance, with many of the fluctuations similar in amplitude to those in the real data. We see that an observed rotation curve with a significant number of "wiggles" is not necessarily a signature of strong patchy absorption, but could also occur in an extremely optically thin galaxy only sparsely populated with H II regions, as is not uncommon in the case of LSB galaxies. Our models suggest that these fluctuations may introduce some additional uncertainty in recovering the precise slope of the inner rotation curve of some LSB galaxies.

5. SUMMARY

We have presented some of the first 3D Monte Carlo simulations of the dusty ISM properties in the low optical depth regimes encountered in low surface brightness (LSB) spiral galaxies. We have demonstrated the power of using such techniques in combination with multiwavelength observational data to constrain the amount and distribution of dust in such systems. Our realistic models fully take into account scattering and the effects of a clumpy, multiphase ISM.

Because late-type LSB galaxies are relatively optically thin, edge-on examples of these systems allow a unique opportunity to explore the structure and distribution of their ISM and place important empirical constraints on dust models. We have shown that while dust contents in LSB galaxies are relatively low, these galaxies can contain modest amounts of dust and molecular material. Moreover, in at least some cases, a significant fraction of this dusty material is contained within a clumpy medium, confirming

that even LSB galaxies can maintain sufficient pressures to support a modest multi-phase ISM structure.

From detailed models of the nearly edge-on LSB galaxy UGC 7321 ($i = 88°$), our Monte Carlo models indicate an edge-on optical depth $\bar{\tau}_{e,B}$ ∼4.0, and hence a total mass of dust is this galaxy of $\sim 8.8 \times 10^5\ \mathcal{M}_\odot$. This is ∼ 20× the warm dust content inferred from *IRAS* 100μm measurements. Total B-band extinction toward the center of this galaxy is estimated to be $\sim 0.43 \pm 0.2$ mag.

We infer that ∼50% of the dusty material in UGC 7321 is contained in a clumpy medium. Based on the detection of CO emission from UGC 7321 by Matthews & Gao (2000), it appears that some fraction of the clumped material is almost certainly molecular gas. However, the dark clouds in LSB galaxies may also contain significant fractions of atomic hydrogen gas. Together our models and direct H I and CO measurements suggest that UGC 7321 has a gas-to-dust ratio of at least 850 in the inner regions of its stellar disk, while the global gas-to-dust ratio for the entire galaxy (including H I gas extending beyond the stellar disk) is estimated to be ∼1600.

In spite of the modest dust contents of LSB galaxies, we have shown that for the range of optical depths expected for such systems, dust extinction will have appreciable effects on the observed total magnitudes and colors only when these galaxies are observed near edge-on. However, even then, the amount of reddening due to dust will be insufficient to explain the large radial color gradients now observed in a number of LSB galaxies (de Blok *et al.* 1996; MGvD99; Matthews *et al.* 2000; Bell *et al.* 2000). Thus some LSB galaxies must have large intrinsic stellar population and/or metallicity gradients in their disks.

We have shown that for realistic optical depths, dust has no appreciable effect on the rotation curves of edge-on spiral galaxies observed in the Hα emission line. Possible holes in the central Hα distributions of such galaxies also cannot fully account for the observed slowly rising rotation curves. Thus the linearly, slowly rising rotation curves seen frequently in many late-type, edge-on or nearly edge-on spirals cannot be fully accounted for by dust and must be due to low central matter densities in these systems. We have demonstrated that in general, projection effects will create a far greater uncertainty than optical depth effects in interpreting the precise intrinsic shapes of the rotation curves of edge-on galaxies.

We thank Mike Wolff for valuable discussions during the course of this work, and KW also thanks Elizabeth Barton and Margaret Geller for many discussions on galaxy rotation curves during the development of the Monte Carlo radiation transfer code that simulates the scattering of emission lines in moving media. LDM is grateful for the support provided by a Jansky Postdoctoral Fellowship from the National Radio Astronomy Observatory. KW acknowledges support from NASA's Long Term Space Astrophysics Research Program (NAG5-6039). The WFPC2 imaging data used for this work were obtained as part of the Wide Field and Planetary Camera 2 Investigation Definition Team science programs. This publication also made use of data products from the Two Micron All Sky Survey, which is a joint project of the University of Massachusetts and the Infrared Processing and Analysis Center/California Institute of Technology, funded by the National Aeronautics and Space Administration and the National Science Foundation.

REFERENCES

Bell, E. F., Barnaby, D., Bower, R. G., de Jong, R. S., Harper, D. A. Jr., Hereld, M., Loewenstein, R. F., & Rauscher, B. J. 2000, MNRAS, 312, 470
Bergvall, N. & Rönnback, J. 1995, MNRAS, 273, 603
Bergvall, N., Rönnback, J., Masegosa, J., Östlin, G. 1999, A&A, 341, 697
Bianchi, S., Ferrara, A., Davies, J. I., & Alton, R. B. 2000, MNRAS, 311, 601
Bianchi, S., Ferrara, A., & Giovanardi, C. 1996, ApJ, 465, 127
Block, D. L., Witt, A. N., Gosbøl, P., Stockton, A., & Moneti, A. 1994, A&A, 288, 383
Boissé, P. 1990, A&A, 228, 483
Bosma, A. 1995, in The Opacity of Spiral Disks, edited by J. I. Davies and D. Burstein, (Dordrecht: Kluwer), p. 317
Bosma, A., Byun, Y., Freeman, K. C., & Athanassoula, E. 1992, ApJ, 400, L21
Bothun, G., Impey, C., & McGaugh, S. 1997, PASP, 109, 745
Bouchet, P., Lequeux, J., Maurice, E., Prévot, L., & Prévot-Burnichon, M. L. 1985, A&A, 149, 330
Byun, Y.-I. 1993, PASP, 105, 993
Carignan, C. 1985, ApJ, 299, 59
Code, A. D. & Whitney, B. A. 1995, ApJ, 441, 400
Cole, A. A., Wood, K., & Nordsieck, K. H. 1999, AJ, 118, 2292
Courteau, S. 1998, AJ, 114, 2402
Cox, P. & Mezger, P. G. 1989, A&ARv, 1, 49
Dalcanton, J. J. & Bernstein, R. A. 2000, in Dynamics of Galaxies: from the Early Universe to the Present, edited by F. COmbes, G. A. Mamon, & V. Charmandaris, (San Francisco: ASP), 161
Dalcanton, J. J. & Schectman, S. A. 1996, ApJ, 465, L9
Davies, J. I. 1991, in Dynamics of Disc Galaxies, edited by B. Sundelius, (Göteborg: Göteborgs University and Chalmers University of Technology), 65
de Blok, W. J. G. & McGaugh, S. S. 1997, MNRAS, 290, 533
de Blok, W. J. G. & van der Hulst, J. M. 1998, A&A, 336, 49
de Blok, W. J. G., van der Hulst, J. M., & Bothun, G. D. 1995, MNRAS, 274, 235
de Grijs, R. 1998, MNRAS, 299, 595
de Jong, R. S. 1996, A&A, 313, 377
Devereux, N. & Young, J. S. 1990, ApJ, 359, 42
Dickey, J. M. 1996, in The Minnesota Lectures on Extragalactic Hydrogen, edited by E. D. Skillman, (San Francisco: ASP), 187
Disney, M., Davies, J., & Phillipps, S. 1989, MNRAS, 239, 939
Dwek, E. 1998, ApJ, 501, 643
Elmegreen, B. G. 1993, in Protostars and Planets III, edited by E. H. Levy and J. I. Lunine, (Tucson: University of Arizona Press), 97
Evans, R. 1994, MNRAS, 266, 511
Ferrara, A., Bianchi, S., Cimatti, A., & Giovanardi, C. 1999, ApJS, 123, 437
Ferrara, A., Bianchi, S., Dettmar, R. -J., & Giovanardi, C. 1996, ApJ, 467, 69
Firmani, C., Hernández, X., & Gallagher, J. S. 1996, A&A, 308, 403
Freeman, K. C. 1970, ApJ, 160, 811
Gallagher, J. S. *et al.* 2000, in prep.
Gerritsen, J. P. E. & de Blok, W. J. G. 1999, A&A, 342, 655
Goad, J. W. & Roberts, M. S. 1981, ApJ, 250, 79
Greenberg, J. M. & Li, A. 1995, in The Opacity of Spiral Disks, edited by J. I. Davies and D. Burstein, (Dordrecht: Kluwer), 19
Han, M. 1992, ApJ, 391, 617
Henyey, L. G. & Greenstein, J. L. 1941, ApJ, 93, 70
Hoeppe, G., Brinks, E., Klein, U., Giovanardi, C., Altschuler, D. R., Price, R. M., & Deeg, H.-J. 1994, AJ, 108, 446
Hoopes, C. G., Walterbos, R. A. M., & Rand, R. J. 1999, ApJ, 522, 669
Howk, J. C. & Savage, B. D. 1999, AJ, 117, 2077
Hunter, D. A., Gallagher, J. S., Rice, W. L., & Gillett, F. C. 1989, ApJ, 336, 152
Impey, C. & Bothun, G. 1997, ARA&A, 35, 267
Jarrett, T. H., Chester, T., Cutri, R., Schneider, S., Skrutskie, M., & Huchra, J. P. 2000, AJ, 119, 2498
Just, A., Fuchs, B., & Wielen, R. 1996, A&A, 309, 715
Karachentsev, I. D., Karachentseva, V. E., & Parnovsky, S. L. 1993, Astron. Nachr., 314, 97
Karachentsev, I. D. & Xu, Z. 1991, Sov. Astron. Lett., 17, 135

Kenney, J. 1997, in The Interstellar Medium of Galaxies, edited by J. M. van der Hulst, (Dordrecht: Kluwer), 33
Kent, S. M. 1986, AJ, 91, 1301
Kim, S. -H., Martin, P. G., & Hendry, P. D. 1994, ApJ, 422, 164
Knezek, P. M. 1993, Ph.D. Thesis, University of Massachusetts
Koorneef, J. 1982, A&A, 107, 247
Kravtsov, A. V., Klypin, A. A., Bullock, J. S., & Primrack, J. R. 1998, ApJ, 502, 48
Kuchinski, L. E. & Terndrup, D. M. 1996, AJ, 111, 1073
Kuchinski, L. E., Terndrup, D. M., Gordon, K. D., & Witt, A. N. 1998, AJ, 115, 1438
Kylafis, N. D. & Bahcall, J. N. 1987, ApJ, 317, 637
Lisenfeld, U. & Ferrara, A. 1998, ApJ, 496, 145
Maloney, P. 1990, in The Interstellar Medium of Galaxies, edited by H. A. Thronson, Jr. & J. M. Shull, (Dordrecht: Kluwer), 493
Makarov, D. I., Burenkov, A. N., & Tyurina, N. V. 1999, Astron. Lett., 25, 706
Makarov, D. I., Karachentsev, I. D., Burenkov, A. N., Tyurina, N. V., & Korotkova, G. G. 1997, Astron. Lett., 23, 638
Mathis, J. S., Rumpl, W., & Nordsieck, K. H. 1977, ApJ, 217, 425
Matthews, L. D. 1998, Ph.D. Thesis, State University of New York at Stony Brook
Matthews, L. D. 2000, AJ, in press
Matthews, L. D. *et al.* 1999, AJ, 118, 208
Matthews, L. D. & Gallagher, J. S. 1997, AJ, 114, 1899
Matthews, L. D., Gallagher, J. S., & van Driel, W. 1999, AJ, 118, 2751 (MGvD99)
Matthews, L. D., Gallagher, J. S., & van Driel, W. 2000, in Galaxy Dynamics: from the Early Universe to the Present, edited by F. Combes, G. A. Mamon, & V. Charmandaris, ASP Conference Series, Vol. 197, (San Francisco: ASP), 195
Matthews, L. D. & Gao. Y. 2000, in prep.
Matthews, L. D. & van Driel, W. 2000, A&AS, 143, 421
Matthews, L. D., van Driel, W., & Gallagher, J. S. 1998, AJ, 116, 2196
McGaugh, S. S. 1994, ApJ, 426, 135
McGaugh, S. S. & de Blok, W. J. G. 1998, ApJ, 499, 41
McGaugh, S. S., Schombert, J. M., Bothun, G. D., & de Blok, W. J. G. 2000, ApJ, 533, 99
McKeith, C. D., Greve, A., Downes, D., & Prada, F. 1995, in The Opacity of Spiral Disks, edited by J. I. Davies and D. Burstein, (Dordrecht: Kluwer), 325
Mihos, J. C., Spaans, M., & McGaugh, S. S. 1999, ApJ, 515, 89
Milgrom, M. 1983, ApJ, 270, 371
Misiriotis, A., Kylafis, N. D., Papamastorakis, J., & Xilouris, E. M. 2000, A&A, 353, 117
O'Neil, K., Bothun, G. D., Impey, C. D., & McGaugh, S. S. 1998, AJ, 116, 657
Pickering, T. E. & van der Hulst, J. M. 1999, AAS, 195, 104.10
Pierni, D. 1999, A&A, 352, 49
Prada, F. 1996, PASP, 108, 549
Prada, F., Beckman, J. E., McKeith, C. D., Castles, J., & Greve, A. 1994, ApJ, 423, L35
Rhee, M.-H. 1996, Ph.D. Thesis, University of Groningen
Rönnback, J. & Bergvall, N. 1995, A&A, 302, 353
Sage, L. J. 1993, A&A, 272, 123
Sancisi, R. & Allen, R. J. 1979, A&A, 74, 73
Sandage, A. & Bedke, J. 1994, The Carnegie Atlas of Galaxies, (Washington: Carnegie Institute of Washington)
Schombert, J. M., Bothun, G. D., Impey, C. D. & Mundy, L. G. 1990, AJ, 100, 1523
Schombert, J. M., Bothun, G. D., Schneider, S. E., & McGaugh, S. S. 1992, AJ, 103, 1107
Spaans, M. 1999, in The Low Surface Brightness Universe, edited by J. I. Davies, C. Impey, & S. Phillips, (San Francisco: ASP), 237
Sprayberry, D. Bernstein, G. M., Impey, C. D., & Bothun, G. D. 1995, ApJ, 438, 72
Stanimirovic, S., Staveley-Smith, L., van der Hulst, J. M., Bontekoe, T. R., Kester, D. J. M., & Jones, P. A. 2000, MNRAS, 315, 791
Stil, J. 1999, Ph.D. Thesis, University of Groningen
Swaters, R. A. 1999, Ph.D. Thesis, University of Groningen
Swaters, R. A., Madore, B. F., & Trewhella, M. 2000, ApJ, 531, L107
Thronson, H. A. & Telesco, C. M. 1986, ApJ, 311, 98
Tielens, A. G. G. M. 1998, ApJ, 499, 267
Trewehella, M., Madore, B., & Kuchinski, L. 1999, in Observational Cosmology: The Development of Galaxy Systems, ASP Conference Series, Vol. 176 (San Francisco: ASP), 454
Tully, R. B., Pierce, M. J., Huang, J.-S., Saunders, W., Verheijen, M. A. W., & Witchalls, P. L. 1998, AJ, 115, 2264
Turner, B. E. 1997, in Astrophysical Implications of the Laboratory Study of Presolar Materials, edited by T. J. Bernatowicz and E. K. Zinner, (Woodbury: American Institute of Physics), 477
Turner, B. E. & Ziurys, L. M. 1988, in Galactic and Extragalactic Radio Astronomy, edited by G. L. Vershuur and K. I. Kellermann, (New York: Springer-Verlag), 200
van den Bosch, F. C. 2000, ApJ, 530, 177
van den Bosch, F. C., Robertson, B. E., Dalcanton, J. J., & de Blok, W. J. G. 2000, AJ, 119, 1579
Wainscoat, R. J., Freeman, K. C., & Hyland, A. R. 1989, ApJ, 337, 163
Whittet, D. C. B. 1992, Dust in the Galactic Environment, (Bristol: IOP Publishing)
Witt, A. N. 1977, ApJS, 35, 1
Witt, A. N. & Gordon, K. D. 1996, ApJ, 463, 681
Witt, A. N. & Gordon, K. D. 2000, ApJ, 528, 799
Witt, A. N., Oliveri, M. V., & Schild, R. E. 1990, AJ, 99, 888
Wood, K. 1997, ApJ, 477, L25
Wood, K. & Jones, T. J. 1997, AJ, 114, 1405
Wood, K. & Reynolds, R. J. 1999, ApJ, 525, 799
Xilouris, E. M., Alton, P. B., Davies, J. I., Kylafis, N. D., Papamastorakis, J., & Trewhella, M. 1998, A&A, 331, 894
Xilouris, E. M., Byun, Y. I., Kylafis, N. D., Paleologou, E. V., & Papamastorakis, J. 1999, A&A, 344, 868
Xilouris, E. M., Kylafis, N. D., Papamastorakis, J., Paleologou, E. V., & Haerendel, G. 1997, A&A, 325, 135
Yusef-Zadeh, F., Morris, M., & White, R. L. 1984, ApJ, 278, 186
Zwaan, M. A., van der Hulst, J. M., de Blok, W. J. G., & McGaugh, S. S. 1995, MNRAS, 273, L35

FIG. 1.— $F702W$+$F814W$ $(R+I)$ composite image of a portion of the disk of UGC 7321, as imaged by the Wide Field and Planetary Camera 2 (WFPC2) aboard the *Hubble Space Telescope*. This is an $55'' \times 19''$ section of the disk, centered near $r = 0$. Resolution is $\sim 0''.1$. White areas reveal the presence of clumpy, optically thick material in the disk of this LSB galaxy.

FIG. 2.— Observed radial $B-R$ color gradient along the major axis of UGC 7321. For ease of comparison with the model computations presented in this paper, the color has been shifted by a constant c_1 such that $(B-R)+c_1 \approx 0$ at the last reliably measured data points, near r =6 kpc. The data were extracted by averaging over a 12-pixel ($2''.3$) wide strip, and smoothed by a factor of 15 for display purposes. For further details see MGvD99.

FIG. 3.— Observed $R-H$ color gradient along the major axis of UGC 7321. The data were extracted by averaging along an $3''$ wide strip and then smoothed by a factor of 3 for display purposes. For ease of comparison with model calculations presented in this paper, the color has been shifted by a constant factor c_2 such that $(R-H)+c_2 \approx 0$ near the last reliable data points at $r = \pm 3.5$ kpc.

FIG. 4.— R-band scattered light images generated from our Monte Carlo simulations of UGC 7321 at $i = 88°$. Each panel is 12.3 kpc is diameter, corresponding to the disk region over which our models were computed. The lefthand column shows models with smooth dust and emissivity distributions, and the righthand column shows models with a 2-phase clumpy ISM and stellar components. Further details on the input parameters for the models are summarized in Sect. 3.1 & 3.2 and Table 2. The four panels in each column represent four different edge-on B-band optical depths: $\tau_{e,B}$=8.0 (top); 4.0 (second row); 2.0 (third row); and 0.4 (bottom).

FIG. 5.— Comparison of our best R- and H-band Monte Carlo model images of UGC 7321 with real data at these wavebands. Top: an R-band image of UGC 7321 obtained with the WIYN telescope by MGvD99 and degraded in resolution to match the resolution of our models ($\sim$60 pc pixel^{-1}. Only the inner 12.3 kpc of the galaxy is shown. Row 2: an R-band model image with $\tau_{e,B}$=4.0 and clumpy ISM and emissivity distributions. Third row: an H-band image of the inner 12.3 kpc of UGC 7321 obtained by MGvD99. Bottom: our model H-band image with $\tau_{e,B}$=4.0 and clumpy ISM and emissivity distributions.

FIG. 6.— Differential $B-R$ and $R-H$ color profiles along the galaxy major axis for our family of $i = 88°$ smooth ISM models (upper panels; see Sect. 3.1) and our clumpy ISM models (lower panels; see Sect. 3.3). Shown are the color difference between models of 4 different edge-on optical depths $\tau_{e,B}$ relative to a zero dust model, as a function of galactocentric distance: $\tau_{e,B} = 8.0$ (solid line); $\tau_{e,B} = 4.0$ (dotted line); $\tau_{e,B} = 2.0$ (dashed line); $\tau_{e,B} = 0.4$ (dot-dash line).

FIG. 7.— Illustration of the origin of the $\Delta(B-R)$ "saturation" effect for a slab model of uniform density and emissivity. Plotted are the color differences in $B-R$ and $R-H$ between a constant density absorbing medium with no scattering and uniform emissivity, and a uniform dust-free emitting medium, as a function of B-band edge-on optical depth τ_B through the slab (see Equation 4). It can be seen that $\Delta(B-R)$ reaches a constant value at a considerably lower optical depth than $\Delta(R-H)$.

FIG. 8.— Differential $H-K$ color profiles along the galaxy major axis for our family of $i = 88°$ clumpy models. Shown are the color difference between models of 4 different optical depths relative to a zero dust model, as a function of galactocentric distance. The 4 different line styles correspond to the same edge-on optical depths as in Figure 6.

FIG. 9.— $H-K_s$ color profile along the major axis of UGC 7321, derived from data from the Two Micron All-Sky Survey (2MASS). The data were extracted by averaging over a 3-pixel wide ($\sim 3''$) strip. The signal-to-noise of the data deteriorate significantly outside the central kpc of the galaxy (see Jarrett *et al.* 2000), but they are consistent with no significant $H-K_s$ color gradient. For ease of comparison with model calculations presented in this paper, the observed color has been shifted by a constant factor c_3 such that $(H-K_s)+c_3 \approx 0$.

FIG. 10.— Dust-induced vertical $B-R$ color gradients, extracted from our clumpy models parallel to the minor axis at three different disk positions. Shown are the color difference between models of 4 different edge-on optical depths $\tau_{e,B}$ relative to a zero dust model, as a function of galactocentric distance: $\tau_{e,B} = 8.0$ (solid line); $\tau_{e,B} = 4.0$ (dotted line); $\tau_{e,B} = 2.0$ (dashed line); $\tau_{e,B} = 0.4$ (dot-dash line). The top panel shows the minor axis color profile; the middle panel shows the color at r=1.5 kpc, and the bottom panel along $r = 3.0$ kpc.

FIG. 11.— Observed $B-R$ vertical color profiles as a function of z (in kpc) for UGC 7321. The data were extracted over 15-pixel ($\sim 3''.0$) wide strips near the minor axis (top) and at r=3.0 kpc (bottom). For display purposes the data were smoothed by a factor of 3. For ease of comparison with the models in Figure 10, the data have been shifted by a constant factor c_4 such that $(B-R)+c_4 \approx 0$ near the last reliably measured data points, at $r = \pm 0.4$ kpc.

FIG. 12.— B-, R-, H-band normalized major axis intensity profiles for our clumpy models viewed at $i = 88°$, with $\bar{\tau}_{e,B}$=0 (thick solid line); 0.4 (dot-dash line); 2.0 (dashed line); 4.0 (dotted line); and 8.0 (solid line).

FIG. 13.— Dust-induced $B-R$ and $R-H$ color gradients as a function of galactocentric radius (in kpc) for smooth models models viewed at inclinations of $i = 0°$, 45°, & 90°. For ease of comparison, the $i = 88°$ smooth models from Figure 6 are also reproduced here. Shown are the color difference between models of 4 different edge-on optical depths $\tau_{e,B}$ relative to a zero dust model, as a function of galactocentric distance: $\tau_{e,B} = 8.0$ (solid line); $\tau_{e,B} = 4.0$ (dotted line); $\tau_{e,B} = 2.0$ (dashed line); $\tau_{e,B} = 0.4$ (dot-dash line).

FIG. 14.— Dust-induced $B-R$ and $R-H$ color gradients as a function of galactocentric radius (in kpc) for clumpy models models viewed at inclinations of $i = 0°$, 45°, & 90°. Line styles are as in Figure 13. For ease of comparison, the $i = 88°$ clumpy models from Figure 6 are also reproduced here.

FIG. 15.— Rotation curves generated from our Monte Carlo models for 3 values of $\tau_{e,B}$ (0, 2, & 100) and 3 viewing angles (i = 85°,88°, & 90°) for the four analytic rotation curve models described in Sect. 4.3.1. Each column shows a different input model. The thick solid line in each panel shows the analytic form of the input rotation curve without any internal extinction. The thin solid line shows the "observed" intensity-weighted rotation curve for the $\tau_{e,B}$=0 (zero dust) model. The dotted line shows the predicted observed curve for a $\tau_{e,B}$=2 model, and the dashed line the predicted observed curve for a $\tau_{e,B}$=100 model. In general, the $\tau_{e,B}$=0 and $\tau_{e,B}$=2 models are nearly indistinguishable.

FIG. 16.— Rotation curves generated from our Monte Carlo models for $\tau_{e,B}$=4.0 and a viewing angle of $i = 88°$. The thick solid line shows the form of the input rotation curve [model (*ii*) (top) and model (*iii*) (bottom; see Text)], and the thin solid line shows the predicted observed rotation curve. Overplotted are datapoints (triangles) measured for UGC 7321 via Hα emission line spectroscopy by Goad & Roberts (1981).

FIG. 17.— Model rotation curves generated for a galaxy seen at $i = 88°$ and devoid of Hα emission over a central hole of radius 1.5 kpc. The thick solid line shows the form of the input rotation curve without any internal extinction. The thin solid line shows the "observed" intensity-weighted rotation curve for the $\tau_{e,B}$=0 (zero dust) model. The dotted line shows the predicted observed curve for a $\tau_{e,B}$=2 model, and the dashed line the predicted observed curve for a $\tau_{e,B}$=100 model. Overplotted are data points (triangles) measured for UGC 7321 by Goad & Roberts (1981) via Hα emission line spectroscopy.

FIG. 18.— Model rotation curves generated for a galaxy seen at $i = 88°$ and having a clumpy distribution of H II regions, with a filling factor $ff_{H\alpha}$=0.005. The thick solid line shows the analytic form of the input rotation curve without any internal extinction. The thin solid line shows the "observed" intensity-weighted rotation curve for the $\tau_{e,B}$=0 (zero dust) model. The dotted line shows the predicted observed curve for a $\tau_{e,B}$=2 model, and the dashed line the predicted observed curve for a $\tau_{e,B}$=100 model. Overplotted are data points (triangles) measured for UGC 7321 via Hα emission line spectroscopy by Goad & Roberts (1981).

arXiv:astro-ph/0010033v1 2 Oct 2000

TABLE 1. Properties of UGC 7321

Hubble type: Sd IV
V_h: 407.2±2.2 (km s^{-1})
Distance: 10^{+3}_{-3} (Mpc)
i : 88°
a/b: 10.3
$D_{25.5}$: 5′.6 (arcmin)
$A_{25.5}$: 16.3 (kpc)
$h_{r,R}$: 43″±4 ≈ 2.1±0.2 (kpc)
$h_{z,H}$: 2″.9±0″.3 ≈ 140 (pc)
m_B: 13.84±0.03
$B-R$: 0.99
$M_{B,i,0}$: −17.05
$\mu_B(0)$: 21.6 (mag arcsec^{-2})
$\mu_{B,i}(0)$: 23.6 (mag arcsec^{-2})
$\bar{\mu}_B$: 27.6 (mag arcsec^{-2})
W_{20}: 233±7 (km s^{-1})
$\mathcal{M}_{HI}$: 1.1×10^9($M_\odot$)
$\mathcal{M}_{HI}/L_B$: 1.1 (solar units)
L_{FIR}: 8×10^7 ($L_\odot$)

Notes to Table 1.

Adopted distance is from J. S. Gallagher (private comm.). The remaining parameters are taken from MGvD99 and Matthews (2000). Apparent magnitude m_B, $B-R$ color, and observed central surface brightness $\mu_B(0)$ have been corrected for Galactic foreground extinction. Absolute B magnitude M_B, mean surface brightness $\bar{\mu}_B$, and extrapolated central surface brightness $\mu_{B,i}(0)$ were corrected for Galactic and internal extinction and projected to face-on values, as described in MGvD99.

arXiv:astro-ph/0010033v1 2 Oct 2000

TABLE 2. Model Input Parameters

λ	κ_λ (cm^2/g)	a_λ	g_λ	C	ff	C_*	ff_*
B	286	0.66	0.59	20	0.06	2	0.60
R	156	0.53	0.40	20	0.06	2	0.60
H	38	0.42	0.29	20	0.06	2	0.60
K	22	0.36	0.25	20	0.06	2	0.60

Notes to Table 2.

Explanation of columns: (1): waveband of the model calculation; (2) opacity of interstellar material; (3) albedo of interstellar grains; (4) phase function asymmetry parameter; (5) density contrast between the clumpy and diffuse ISM (clumpy models only); (6) filling factor of the ISM clumps (clumpy models only); (7) density contrast between clumped and smooth emissivity (clumpy models only); (8) filling factor of the clumpy emission (clumpy models only). For all models discussed in this paper: $h_{r,*}$ =2.1 kpc, $h_{z,*}$=140 pc, $h_{r,d}$=1.5 kpc; $h_{z,d}$=70 pc, and both the dust and the stars were assumed to follow exponential vertical and radial distributions (see Sect. 2).